SANDIA REPORT

SAND2007-8104
Unlimited Release
Printed December 2007

Lagrangian Continuum Dynamics in ALEGRA

E. Love, Sandia
M. K. Wong, Sandia

Prepared by
Sandia National Laboratories
Albuquerque, New Mexico 87185 and Livermore, California 94550

Sandia is a multiprogram laboratory operated by Sandia Corporation,
a Lockheed Martin Company, for the United States Department of Energy's
National Nuclear Security Administration under Contract DE-AC04-94-AL85000.

Issued by Sandia National Laboratories, operated for the United States Department of Energy by Sandia Corporation.

Available to DOE and DOE contractors from
U.S. Department of Energy
Office of Scientific and Technical Information
P.O. Box 62
Oak Ridge, TN 37831

Telephone: (865) 576-8401
Facsimile: (865) 576-5728
E-Mail: reports@adonis.osti.gov
Online ordering: http://www.doe.gov/bridge

Available to the public from
U.S. Department of Commerce
National Technical Information Service
5285 Port Royal Rd
Springfield, VA 22161

Telephone: (800) 553-6847
Facsimile: (703) 605-6900
E-Mail: orders@ntis.fedworld.gov
Online ordering: http://www.ntis.gov/ordering.htm

SAND2007-8104
Unlimited Release
Printed December 2007

Lagrangian Continuum Dynamics in ALEGRA

E. Love and M. K. Wong
Computational Shock- and Multi-physics Department
Sandia National Laboratories
P.O. Box 5800, MS 0378
Albuquerque, NM 87185-0378, USA
elove@sandia.gov
mkwong@sandia.gov

Abstract

ALEGRA is an ALE (Arbitrary Lagrangian-Eulerian) multi-material finite element code that emphasizes large deformations and strong shock physics. The Lagrangian continuum dynamics package in ALEGRA uses a Galerkin finite element spatial discretization and an explicit central-difference stepping method in time. The goal of this report is to describe in detail the characteristics of this algorithm, including the conservation and stability properties. The details provided should help both researchers and analysts understand the underlying theory and numerical implementation of the ALEGRA continuum hydrodynamics algorithm.

This page intentionally left blank.

Contents

Appendix

This page intentionally left blank.

Lagrangian Continuum Dynamics in ALEGRA

List of Notation and Symbols

$(\cdot) \bullet (\cdot)$	dot product in any finite dimensional real vector space, see equation (20), page 14.
$(\cdot) \circ (\cdot)$	operator composition, see equation (7), page 12.
$< \cdot, \cdot >$	L^2 inner product, see equation (20), page 14.
α, β	time integration parameters $\in [0, 1]$.
$\bar{(\cdot)}$	mean value of $(\cdot)$, see equation (62), page 20.
$\mathbf{a}$	spatial material acceleration, see equation (8), page 13.
$\mathbf{b}$	body force density per unit mass, see equation (22), page 14.
$\mathbf{C}$	right Cauchy-Green strain tensor, see equation (6), page 12.
$\mathbf{D}$	material rate of deformation tensor, see equation (11), page 13.
$\mathbf{d}$	rate of deformation tensor, see equation (10), page 13.
$\mathbf{F}$	deformation gradient, see equation (4), page 12.
$\mathbf{g}$	spatial metric tensor, see equation (102), page 30.
$\mathbf{I}$	rank-two identity tensor, see equation (102), page 30.
$\mathbf{l}$	velocity gradient, see equation (9), page 13.
$\mathbf{P}$	first Piola-Kirchhoff stress, see equation (16), page 13.
$\mathbf{Q}$	arbitrary rotation tensor.
$\mathbf{q}$	spatial (Cauchy) heat flux, see equation (92), page 27.
$\mathbf{R}$	polar decomposition rotation, see equation (4), page 12.
$\mathbf{S}$	second (symmetric) Piola-Kirchhoff stress, see equation (15), page 13.
$\mathbf{t}$	surface traction, see equation (22), page 14.
$\mathbf{u}$	incremental displacement field, see equation (30), page 15.
$\mathbf{V}$	left stretch tensor, see equation (4), page 12.
$\mathbf{v}$	spatial material velocity, see equation (7), page 12.
$\mathbf{w}$	skew part of velocity gradient, see equation (12), page 13.
$\mathbf{X}$	a point of the material domain, page 11.
$\mathbf{x}$	a point of the spatial domain, page 11.
$\mathbf{\Omega}$	rate of change of polar decomposition rotation tensor, see equation (13), page 13.
$\mathbf{\Sigma}$	rotated Cauchy stress, see equation (17), page 13.
$\boldsymbol{\sigma}$	Cauchy stress, see equation (15), page 13.

$\mathbf{x}_i$	vector of nodal coordinates for component i, see equation (115), page 33.
$\boldsymbol{\sigma}_{\text{visc}}$	artificial viscous stress, see equation (97), page 29.
$\boldsymbol{\tau}$	Kirchhoff stress, see equation (18), page 13.
$\delta\boldsymbol{\varphi}$	kinematically admissible virtual displacement field, see equation (22), page 14.
$\det(\cdot)$	determinant of $(\cdot)$, see equation (5), page 12.
$\text{DEV}(\cdot)$	$\boldsymbol{\varphi}^*[\text{dev}\,\boldsymbol{\varphi}_*(\cdot)]$, see equation (144), page 44.
$\mathbf{U}$	total displacement field, see equation (35), page 16.
$\dot{(\cdot)}$	material time derivative of $(\cdot)$, see equation (7), page 12.
η	internal entropy density, see equation (88), page 27.
$\exp(\cdot)$	exponential of $(\cdot)$, see equation (105), page 30.
Γ	boundary of the domain, see equation (3), page 12.
$\text{grad}(\cdot)$	spatial gradient of $(\cdot)$, see equation (22), page 14.
$\boldsymbol{\phi}$	incremental motion, see equation (29), page 15.
$\mathcal{L}_{\mathbf{v}}[\cdot]$	Lie derivative of $[\cdot]$, see equation (102), page 30.
$\log(\cdot)$	logarithm of $(\cdot)$, see equation (107), page 31.
$\mathbb{C}$	rank-4 constitutive tensor, see equation (84), page 25.
$\mathcal{H}$	hourglass functions, see equation (112), page 33.
$\mathcal{R}$	external heat source, see equation (93), page 27.
$\boldsymbol{\varphi}$	motion of the body, see equation (1), page 12.
$\boldsymbol{\varphi}^*(\cdot)$	pull-back of $(\cdot)$, see equation (100), page 30.
$\boldsymbol{\varphi}_*(\cdot)$	push-forward of $(\cdot)$, see equation (100), page 30.
Ω	spatial configuration of the body, see equation (3), page 12.
Ω_0	material configuration of the body, see equation (1), page 12.
$\text{div}(\cdot)$	spatial divergence of $(\cdot)$, see equation (92), page 27.
Ψ	Helmholtz free-energy density, see equation (86), page 26.
ρ	spatial mass density, see equation (14), page 13.
ρ_0	material mass density, see equation (14), page 13.
h	time step, see equation (36), page 16.
p	spatial (Cauchy) pressure, positive in compression, see equation (65), page 22.
t	time.
$\text{skew}(\cdot)$	skew part of $(\cdot)$, see equation (12), page 13.
$\overset{\triangledown}{\boldsymbol{\sigma}}$	objective stress rate, see equation (19), page 13.
$\text{symm}(\cdot)$	symmetric part of $(\cdot)$, see equation (10), page 13.
Θ	absolute temperature, see equation (86), page 26.

$\mathrm{trace}(\cdot)$	trace of $(\cdot)$, see equation (95), page 28.
ε	internal energy density per unit mass, see equation (25), page 14.
ξ	element natural coordinates, see equation (110), page 32.
c_s	material sound speed, see equation (98), page 29.
h_e	element characteristic length scale, see equation (124), page 34.
J	determinant of deformation gradient (volume element), see equation (5), page 12.
j	determinant of incremental deformation gradient (incremental volume element), see equation (33), page 15.
N^A	shape function for node A, see equation (57), page 19.
r	external heat source per unit mass, see equation (25), page 14.
$SO(3)$	special orthogonal group.
$(\cdot)^{\mathrm{pred}}$	predicted value of $(\cdot)$, see equation (39), page 16.
$(\cdot)_{\mathrm{n}+\alpha}$	quantity $(\cdot)$ at time $\mathrm{t}_{\mathrm{n}+\alpha}$, see equation (27), page 15.
$(\cdot)^s$	symmetric part of $(\cdot)$, see equation (22), page 14.
$\mathbf{a}_c$	contact induced acceleration, see equation (42), page 16.
$\mathbf{b}_i$	nodal 'strain-displacement' vector for component i, see equation (118), page 33.
$\mathbf{F}^A_{\mathrm{ext}}$	external force vector at node A, see equation (61), page 20.
$\mathbf{F}^A_{\mathrm{int}}$	internal force vector at node A, see equation (60), page 20.
$\mathbf{F}^{hg}_m$	nodal forces for hourglass mode m, see equation (133), page 36.
$\mathbf{f}^{hg}_m$	hourglass resistance for mode m, see equation (123), page 34.
$\mathbf{h}_j$	hourglass vector for mode j, see equation (115), page 33.
$\mathbf{id}$	the identity mapping, see equation (28), page 15.
$\mathbf{N}(\boldsymbol{\xi})$	vector of element shape functions, see equation (110), page 32.
$\mathbf{r}^{hg}_m$	hourglass rate for mode m, see equation (123), page 34.
$\mathbf{s}^{hg}_m$	Pronto hourglass stiffness parameter for mode m, see equation (131), page 35.
$\mathbf{t}_c$	contact induced traction, see equation (42), page 16.
T	total kinetic energy, see equation (73), page 23.
V	total internal energy, see equation (74), page 23.
$\mathbf{f}$	incremental deformation gradient, see equation (32), page 15.

This page intentionally left blank.

1 Introduction

ALEGRA [20, 99, 109] was originally developed as an ALE (Arbitrary Lagrangian-Eulerian) multi-material finite element code that emphasizes large deformations and strong shock physics. As an effort to combine the modeling features of modern Eulerian shock codes with the improved numerical accuracy of modern Lagrangian finite element codes, ALEGRA is based on and follows the approach of the Pronto transient dynamics code [62, 100] and contains elements of the CTH family of shock wave codes [59, 74]. This capability permits a calculation to proceed in Lagrangian fashion until portions of the finite element mesh become highly distorted, at which time the nodal points in the most deformed portion of the mesh are moved to reduce the distortion to acceptable levels. This remeshing prevents the mesh from distorting to the point where accuracy is lost. The remeshing is limited to only those regions where severe distortions require mesh movement. In addition to mesh smoothing, the ALEGRA remesh algorithm can also move nodes to better resolve mesh regions with specific values of selected variables or their gradients. The ALEGRA remesh and remap capabilities are described in [36, 81].

ALEGRA has more recently become a general purpose multi-physics simulation software package, with a focus on Z-pinch experiments [43, 66, 84] and Army Research Laboratory advanced armor simulations [65]. The performance of ALEGRA on general multi-physics problems is in large part dependent upon the performance and characteristics of the Lagrangian finite element algorithm. The goal of this report is to describe in detail the characteristics of this algorithm, including the conservation and stability properties. The details provided should help both researchers and analysts understand the underlying theory and numerical implementation of the ALEGRA continuum hydrodynamics algorithm. Although ALEGRA now has many multi-physics extensions [19, 89] (magnetics, two-temperature plasma physics and radiation), attention here is specifically focused upon single-material continuum thermo-mechanical problems.

The outline of the report is as follows. Section 2 provides a brief review of continuum mechanics. The presentation in this section is very terse, and the reader with a working knowledge of continuum mechanics will much more easily understand the material. In this regard the references noted provide invaluable background material. Section 3 describes the time-integration algorithm for the momentum balance equation. ALEGRA uses what is known as the *central-difference method*. Section 4 describes some details of the spatial interpolation scheme. Section 5 reviews the time-integration algorithm for the energy update equation, and also includes a discussion of conservation and stability properties. Section 6 presents the time-discrete method for updating the stress response of the material models being used. The discussion includes both hypo- and hyper- elastic material models. Section 7 reviews the shock capturing algorithm used and Section 8 discusses the hourglass control algorithm. A shock capturing method introduces artificial entropy production and is needed to correctly model the dissipation produced by the presence of strong discontinuities. An hourglass control algorithm is designed to help ensure stability of the numerical formulation in the presence of reduced, less accurate spatial quadrature rules. Finally, some brief concluding remarks are made in Section 9. An appendix is included to present some additional specific details not directly needed in the main report content.

2 Continuum Mechanics

For a comprehensive review of continuum (thermo)mechanics, the reader may consult [1, 28, 47, 71, 79, 104]. For a more introductory presentation, oriented towards finite element analysis, the reader may consult [13, 27, 53].

2.1 Kinematics

Let $\Omega_0 \subsetneq \mathbb{R}^3$ denote the reference (material) configuration of a continuum body, with material points labeled $\mathbf{X}$. The set Ω_0 is open, bounded $\text{meas}(\Omega_0) < \infty$, and has a smooth boundary. Let the spatial (current) configuration of the same body be $\Omega_t \subsetneq \mathbb{R}^3$, with points labeled $\mathbf{x}$. Assume there exists a smooth mapping, the motion of the body,

$$\boldsymbol{\varphi} : \Omega_0 \times [0, T] \longmapsto \mathbb{R}^3 \ , \tag{1}$$

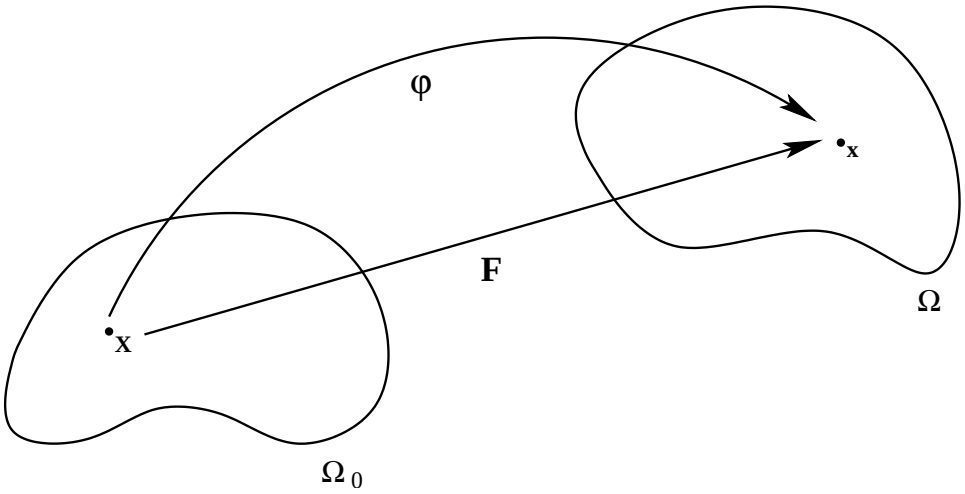

Figure 1. Kinematics of motion of a deforming body.

or equivalently,

$$\boldsymbol{\varphi}_{\mathrm{t}} : \Omega_0 \longmapsto \mathbb{R}^3 \ , \tag{2}$$

such that

$$\Omega_{\mathrm{t}} := \boldsymbol{\varphi}_{\mathrm{t}}(\Omega_0) \ , \tag{3}$$

and $\mathbf{x} = \boldsymbol{\varphi}(\mathbf{X}, \mathrm{t}) = \boldsymbol{\varphi}_{\mathrm{t}}(\mathbf{X})$, where $[0, T]$ is the time interval of interest. Figure 1 provides a visual representation of these kinematic assumptions. The boundary of Ω_{t} is defined as

$$\Gamma_{\mathrm{t}} := \overline{\Omega_{\mathrm{t}}} \bigcap \overline{\mathbb{R}^3 \setminus \Omega_{\mathrm{t}}} \ .$$

This boundary is assumed to be partitioned into disjoint subsets such that

$$\Gamma_{\mathrm{t}} = \overline{\Gamma_{\mathbf{u}} \bigcup \Gamma_{\boldsymbol{\sigma}}} \quad \text{and} \quad \Gamma_{\mathbf{u}} \bigcap \Gamma_{\boldsymbol{\sigma}} = \emptyset \ .$$

The traction $\bar{\mathbf{t}} : \Gamma_{\boldsymbol{\sigma}} \longmapsto \mathbb{R}^3$ is prescribed on the Neumann boundary $\Gamma_{\boldsymbol{\sigma}}$ and velocity (or displacement) is prescribed on the Dirichlet boundary $\Gamma_{\mathbf{u}}$.

Consistent with this construction, define

$$\mathbf{F}_{\mathrm{t}} = D\boldsymbol{\varphi}_{\mathrm{t}} = \mathrm{GRAD}_{\mathbf{X}}[\boldsymbol{\varphi}] = \mathbf{V}_{\mathrm{t}}\mathbf{R}_{\mathrm{t}} \tag{4}$$

as the deformation gradient of the motion, with volume element

$$J_{\mathrm{t}} = \det[\mathbf{F}_{\mathrm{t}}] \ . \tag{5}$$

The tensors $\mathbf{V}$ and $\mathbf{R}$ are the stretch and rotation, respectively, associated with the polar decomposition of $\mathbf{F}$. Define

$$\mathbf{C}_{\mathrm{t}} = \mathbf{F}_{\mathrm{t}}^T \mathbf{F}_{\mathrm{t}} \tag{6}$$

as the right Cauchy-Green strain tensor.

The spatial material velocity is computed as

$$\mathbf{v}_{\mathrm{t}} = \dot{\boldsymbol{\varphi}}_{\mathrm{t}} \circ \boldsymbol{\varphi}_{\mathrm{t}}^{-1} \ , \tag{7}$$

where the superimposed dot denotes the material time derivative (time derivative holding $\mathbf{X}$ fixed). The spatial material acceleration is

$$\mathbf{a}_{\mathrm{t}} = \ddot{\boldsymbol{\varphi}}_{\mathrm{t}} \circ \boldsymbol{\varphi}_{\mathrm{t}}^{-1} \ . \tag{8}$$

Some material models require deformation rate(s) to evaluate their stress response. Towards that end, define

$$\mathbf{l}_{\mathrm{t}} = \mathrm{grad}[\mathbf{v}_{\mathrm{t}}] = \left(\dot{\mathbf{F}}_{\mathrm{t}}\mathbf{F}_{\mathrm{t}}^{-1}\right) \circ \boldsymbol{\varphi}_{\mathrm{t}}^{-1} \ , \tag{9}$$

as the spatial velocity gradient and

$$\mathbf{d}_{\mathrm{t}} = \mathrm{symm}[\mathbf{l}_{\mathrm{t}}] \ , \tag{10}$$

as the spatial rate of deformation tensor. The spatial rate of deformation tensor $\mathbf{d}$ may be rotated back to the material configuration via the transformation

$$\mathbf{D}_{\mathrm{t}} = \mathbf{R}_{\mathrm{t}}^{T} \left(\mathbf{d}_{\mathrm{t}} \circ \boldsymbol{\varphi}_{\mathrm{t}}\right) \mathbf{R}_{\mathrm{t}} \ , \tag{11}$$

thus defining a material rate of deformation tensor. Materials typically undergo both stretch and rotation and multiple rotation rates may be constructed. For the purposes of this report, define two rotation rates

$$\mathbf{w}_{\mathrm{t}} = \mathrm{skew}[\mathbf{l}_{\mathrm{t}}] \ , \tag{12}$$

and

$$\boldsymbol{\Omega}_{\mathrm{t}} = \left(\dot{\mathbf{R}}_{\mathrm{t}}\mathbf{R}_{\mathrm{t}}^{T}\right) \circ \boldsymbol{\varphi}_{\mathrm{t}}^{-1} \iff \dot{\mathbf{R}}_{\mathrm{t}} = \left(\boldsymbol{\Omega}_{\mathrm{t}} \circ \boldsymbol{\varphi}_{\mathrm{t}}\right) \mathbf{R}_{\mathrm{t}} \ . \tag{13}$$

Note that these two rates are in general not the same for arbitrary motions.

2.2 Kinetics

The law of conservation of mass may be written quite simply as follows. Given a material mass density $\rho_0 : \Omega_0 \longmapsto \mathbb{R}^+$, the spatial mass density $\rho_{\mathrm{t}} : \Omega_{\mathrm{t}} \longmapsto \mathbb{R}^+$ is given by

$$\rho_{\mathrm{t}} = \left(J_{\mathrm{t}}^{-1}\rho_0\right) \circ \boldsymbol{\varphi}_{\mathrm{t}}^{-1} \ . \tag{14}$$

Let $\boldsymbol{\sigma}_t : \Omega_{\mathrm{t}} \longmapsto \mathbb{R}^6$ denote the symmetric Cauchy stress in the current configuration. Then define

$$\mathbf{S}_{\mathrm{t}} = J_{\mathrm{t}}\mathbf{F}_{\mathrm{t}}^{-1} \left(\boldsymbol{\sigma}_t \circ \boldsymbol{\varphi}_{\mathrm{t}}\right) \mathbf{F}_{\mathrm{t}}^{-T} \ , \tag{15}$$

as the second (symmetric) Piola-Kirchhoff stress,

$$\mathbf{P}_{\mathrm{t}} = \mathbf{F}_{\mathrm{t}}\mathbf{S}_{\mathrm{t}} \ , \tag{16}$$

as the first, and generally unsymmetric, Piola-Kirchhoff stress and

$$\boldsymbol{\Sigma}_{\mathrm{t}} = \mathbf{R}_{\mathrm{t}}^{T} \left(\boldsymbol{\sigma}_t \circ \boldsymbol{\varphi}_{\mathrm{t}}\right) \mathbf{R}_{\mathrm{t}} \ , \tag{17}$$

as the Cauchy stress rotated back to the material configuration. In many situations it proves convenient to work with the Kirchhoff stress

$$\boldsymbol{\tau}_{\mathrm{t}} := J_{\mathrm{t}}\boldsymbol{\sigma}_{\mathrm{t}} = \mathbf{F}_{\mathrm{t}}\mathbf{S}_{\mathrm{t}}\mathbf{F}_{\mathrm{t}}^{T}. \tag{18}$$

Many *hypo-elastic* material models in ALEGRA are based upon the use of the Green-McInnis-Naghdi [96] objective stress rate

$$\overset{\triangledown}{\boldsymbol{\sigma}} := \left(\mathbf{R}_{\mathrm{t}} \left[\frac{\mathrm{d}}{\mathrm{dt}}\boldsymbol{\Sigma}_{\mathrm{t}}\right] \mathbf{R}_{\mathrm{t}}^{T}\right) \circ \boldsymbol{\varphi}_{\mathrm{t}}^{-1} \ . \tag{19}$$

Remarks 2.1.

1. The Green-McInnis-Naghdi rate is simply one rate among many. All objective rates are essentially Lie derivatives [71]. Hypo-elastic material models require the use of an objective stress rate. However, the choice of which rate to use is a matter of personal preference or computational convenience. There are no formal mathematical or rational thermodynamic reasons to prefer one rate over another.

2. Reference [104], footnote, page 404: "Various stress rates have been used in the literature. Despite claims and whole papers to the contrary, any advantage claimed for one such rate over another is pure illusion."

It proves convenient at this juncture to introduce the L^2 inner product(s) as

$$\langle \mathbf{a}, \mathbf{b} \rangle_{\mathrm{t}} = \int_{\Omega_{\mathrm{t}}} \mathbf{a} \bullet \mathbf{b} \, \mathrm{d}\Omega_{\mathrm{t}} \ , \tag{20}$$

$$\langle \mathbf{a}, \mathbf{b} \rangle_{\Gamma} = \int_{\Gamma} \mathbf{a} \bullet \mathbf{b} \, \mathrm{d}\Gamma \ . \tag{21}$$

With this notation in hand, the weak form of the balance of linear momentum may be written as: find $\boldsymbol{\varphi}$ satisfying the boundary conditions on $\Gamma_{\mathbf{u}}$ such that for all $\delta\boldsymbol{\varphi}$

$$\langle \delta\boldsymbol{\varphi}, \rho_{\mathrm{t}} \mathbf{a}_{\mathrm{t}} \rangle_{\mathrm{t}} + \Big\langle \mathrm{grad}^{(s)} \, \delta\boldsymbol{\varphi}, \boldsymbol{\sigma}_{\mathrm{t}} \Big\rangle_{\mathrm{t}} - \langle \delta\boldsymbol{\varphi}, \rho_{\mathrm{t}} \mathbf{b} \rangle_{\mathrm{t}} - \langle \delta\boldsymbol{\varphi}, \bar{\mathbf{t}} \rangle_{\Gamma_{\boldsymbol{\sigma}}} = 0 \ \ , \tag{22}$$

where $\mathbf{b}$ is the body-force density per unit mass and $\bar{\mathbf{t}}$ is the prescribed traction on the Neumann boundary $\Gamma_{\boldsymbol{\sigma}}$. The notation $(\cdot)^s$ or $(\cdot)^{(s)}$ indicates the symmetric part of $(\cdot)$. This is often referred to as the principle of virtual work in the spatial configuration [28]. The virtual displacement field $\delta\boldsymbol{\varphi}$ is required to be *kinematically admissible* in the sense that $\delta\boldsymbol{\varphi}$ vanishes on the Dirichlet boundary $\Gamma_{\mathbf{u}}$. Equation (22) is equivalent to

$$\langle \delta\boldsymbol{\varphi}, \rho_0 \mathbf{a}_{\mathrm{t}} \rangle_0 + \langle \mathrm{GRAD}_{\mathbf{X}} \, \delta\boldsymbol{\varphi}, \mathbf{P}_{\mathrm{t}} \rangle_0 - \langle \delta\boldsymbol{\varphi}, \rho_0 \mathbf{b} \rangle_0 - \big\langle \delta\boldsymbol{\varphi}, \bar{\mathbf{T}} \big\rangle_{\Gamma^0_{\boldsymbol{\sigma}}} = 0 \ , \tag{23}$$

where $\bar{\mathbf{T}} \cdot \mathrm{d}\Gamma^0 := \bar{\mathbf{t}} \cdot \mathrm{d}\Gamma_{\mathrm{t}}$, $\Gamma^0 := \boldsymbol{\varphi}_{\mathrm{t}}^{-1}(\Gamma_{\mathrm{t}})$ and $\Gamma^0_{\boldsymbol{\sigma}} := \boldsymbol{\varphi}_t^{-1}(\Gamma_{\boldsymbol{\sigma}})$. This is the principle of virtual work in the reference (material) configuration [28].

Remarks 2.2. Nansen's formula [28, 47, 71] states that

$$\mathbf{n} \cdot \mathrm{d}\Gamma_{\mathrm{t}} = J_{\mathrm{t}} \mathbf{F}_{\mathrm{t}}^{-T} \mathbf{N} \cdot \mathrm{d}\Gamma^0 \ , \tag{24}$$

where $\mathbf{n}$ and $\mathbf{N}$ are the unit outward normals to the spatial and material configurations, respectively.

2.3 Balance of energy

Assume there exists an internal energy density function (per unit mass) $\varepsilon : \Omega_{\mathrm{t}} \longrightarrow \mathbb{R}^+$. The spatial balance of energy equation is ([104], equation 79.3)

$$\rho_{\mathrm{t}} \dot{\varepsilon} = (\boldsymbol{\sigma}_{\mathrm{t}} \bullet \mathbf{d}_{\mathrm{t}}) - \mathrm{div} \, \mathbf{q} + \rho_{\mathrm{t}} r \ , \tag{25}$$

where $\mathbf{q} : \Omega_{\mathrm{t}} \longrightarrow \mathbb{R}^3$ is the spatial (Cauchy) heat flux and $r : \Omega_{\mathrm{t}} \longrightarrow \mathbb{R}$ is the external heat source per unit mass.

3 Discrete Time Integration

For a comprehensive overview of the time-stepping and stress update algorithms used in finite element hydrocodes the reader is strongly encouraged to review [10]. The notation used in this section is almost exactly that of Section 8.1 of [96].

3.1 Incremental kinematics

The goal of this subsection is to describe the time-discrete kinematics used in Alegra . Define the midpoint configuration of the body as the convex combination

$$\boldsymbol{\varphi}_{\mathrm{n}+\alpha} = (1-\alpha)\boldsymbol{\varphi}_{\mathrm{n}} + \alpha \boldsymbol{\varphi}_{\mathrm{n}+1} \quad \text{for } \alpha \in [0,1] \ . \tag{26}$$

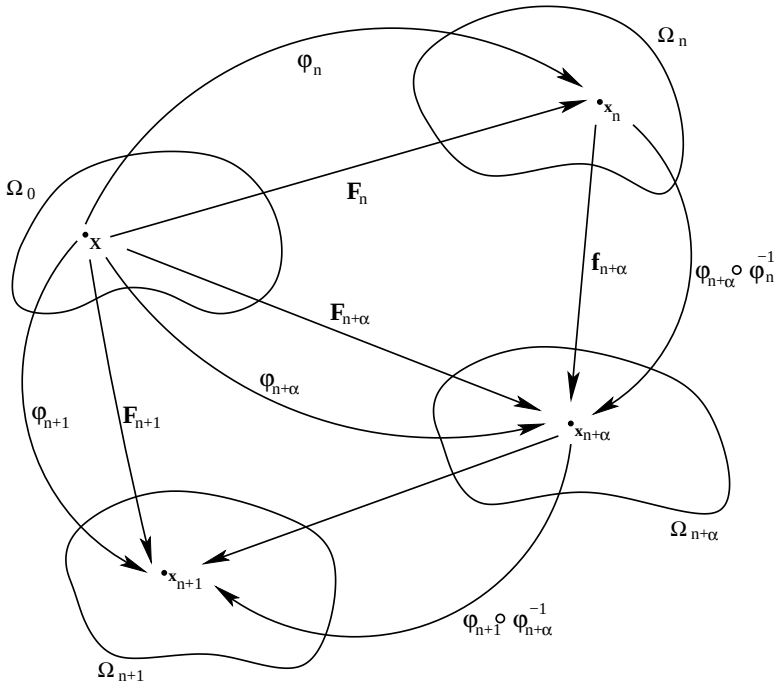

Figure 2. Incremental kinematics of motion of a deforming body.

Consistent with this, the midpoint deformation gradient is the convex combination

$$\mathbf{F}_{\mathrm{n}+\alpha} = (1-\alpha)\mathbf{F}_{\mathrm{n}} + \alpha\mathbf{F}_{\mathrm{n}+1} \quad \text{for } \alpha \in [0,1] \; . \tag{27}$$

The incremental motion relating the configurations Ω_{n} and $\Omega_{\mathrm{n}+1}$ is

$$\boldsymbol{\phi} = \boldsymbol{\varphi}_{\mathrm{n}+1} \circ \boldsymbol{\varphi}_{\mathrm{n}}^{-1} = \mathbf{id} + \mathbf{u}_{\mathrm{n}+1} \; , \tag{28}$$

where **id** is the identity mapping. By this construction

$$\boldsymbol{\phi} : \Omega_{\mathrm{n}} \longrightarrow \Omega_{\mathrm{n}+1} \; . \tag{29}$$

The incremental displacement field is defined as

$$\mathbf{u}_{\mathrm{n}+1} = (\boldsymbol{\varphi}_{\mathrm{n}+1} - \boldsymbol{\varphi}_{\mathrm{n}}) \circ \boldsymbol{\varphi}_{\mathrm{n}}^{-1} \; . \tag{30}$$

The displacement field $\mathbf{u}_{\mathrm{n}+1}$ can be evaluated as a function of $\mathbf{x}_{\mathrm{n}}$ or as a function of $\mathbf{x}_{\mathrm{n}+\alpha}$ using the operator compositions

$$\tilde{\mathbf{u}}_{\mathrm{n}+1} := \mathbf{u}_{\mathrm{n}+1} \circ \boldsymbol{\varphi}_{n} \circ \boldsymbol{\varphi}_{\mathrm{n}+\alpha}^{-1} = (\boldsymbol{\varphi}_{\mathrm{n}+1} - \boldsymbol{\varphi}_{\mathrm{n}}) \circ \boldsymbol{\varphi}_{\mathrm{n}+\alpha}^{-1} \; . \tag{31}$$

Figure 2 provides a visual representation of these incremental kinematics.

The incremental deformation gradient is defined as

$$\mathbf{f}_{\mathrm{n}+\alpha} = \mathrm{grad}_{\mathrm{n}}[\boldsymbol{\varphi}_{\mathrm{n}+\alpha} \circ \boldsymbol{\varphi}_{\mathrm{n}}^{-1}] = \mathbf{F}_{\mathrm{n}+\alpha}\mathbf{F}_{\mathrm{n}}^{-1} \; , \tag{32}$$

with an incremental volume element

$$j_{\mathrm{n}+\alpha} = \det[\mathbf{f}_{\mathrm{n}+\alpha}] \; . \tag{33}$$

To compute this deformation from the incremental displacement field, notice that

$$\mathbf{f}_{\mathrm{n}+\alpha} = (1-\alpha)\mathbf{I} + \alpha\mathbf{f}_{\mathrm{n}+1} = \mathbf{I} + \alpha\,\mathrm{grad}_{\mathrm{n}}[\mathbf{u}_{\mathrm{n}+1}] \; . \tag{34}$$

It is possible to accumulate the total displacement field, if desired. This field is simply the accumulated sum

$$\mathsf{U}_{\mathrm{n}+1} := \boldsymbol{\varphi}_{\mathrm{n}+1} - \boldsymbol{\varphi}_0 = \sum_{i=0}^{\mathrm{n}} (\boldsymbol{\varphi}_{i+1} - \boldsymbol{\varphi}_i) = \sum_{i=0}^{\mathrm{n}} \mathbf{u}_{i+1} \circ \boldsymbol{\varphi}_i \tag{35}$$

There are at least two ways to compute the total deformation using the total displacement field:

1.
$$\mathbf{F}_{\mathrm{n}+1} = \mathbf{I} + \mathrm{GRAD}_{\mathbf{X}}[\mathsf{U}_{\mathrm{n}+1}]$$

2.
$$\mathbf{F}_{\mathrm{n}+1}^{-1} = \mathbf{I} - \mathrm{grad}_{\mathrm{n}+1}[\mathsf{U}_{\mathrm{n}+1} \circ \boldsymbol{\varphi}_{\mathrm{n}+1}^{-1}]$$

3.
$$\mathbf{F}_{\mathrm{n}+\alpha} = \mathrm{GRAD}_{\mathbf{X}}[\boldsymbol{\varphi}_{\mathrm{n}+\alpha}] = (1-\alpha)\mathbf{F}_{\mathrm{n}} + \alpha \mathbf{F}_{\mathrm{n}+1}$$

3.2 Central-Difference Method

ALEGRA uses the *central-difference method* to integrate in time the continuum dynamics equation(s) of motion. For more detailed information, the reader may consult [7, 62, 110]. Given data $\{\mathsf{U}_{\mathrm{n}}, \mathbf{v}_{\mathrm{n}-1/2}, \boldsymbol{\sigma}_{\mathrm{n}}, \varepsilon_{\mathrm{n}}\}$, the goal is to compute $\{\mathbf{u}_{\mathrm{n}+1}, \mathsf{U}_{\mathrm{n}+1}, \mathbf{v}_{\mathrm{n}+1/2}, \boldsymbol{\sigma}_{\mathrm{n}+1}, \varepsilon_{\mathrm{n}+1}\}$. The time step(s) are defined as

$$\left.\begin{aligned} \mathrm{h}_{\mathrm{n}+1} &= \mathrm{t}_{\mathrm{n}+1} - \mathrm{t}_{\mathrm{n}}; \\ \mathrm{h}_{\mathrm{n}} &= \mathrm{t}_{\mathrm{n}} - \mathrm{t}_{\mathrm{n}-1}; \\ \bar{\mathrm{h}} &= \frac{1}{2}(\mathrm{h}_{\mathrm{n}} + \mathrm{h}_{\mathrm{n}+1}) \end{aligned}\right\} . \tag{36}$$

Algorithm Central-Difference. The central-difference method is implemented in eight(8) steps:

1. Solve for the accelerations:

$$\langle \delta\boldsymbol{\varphi}, \rho_{\mathrm{n}} \mathbf{a}_{\mathrm{n}} \rangle_{\mathrm{n}} + \left\langle \mathrm{grad}_{\mathrm{n}}^{(s)}[\delta\boldsymbol{\varphi}], \boldsymbol{\sigma}_{\mathrm{n}} \right\rangle_{\mathrm{n}} - \langle \delta\boldsymbol{\varphi}, \rho_{\mathrm{n}} \mathbf{b} \rangle_{\mathrm{n}} - \langle \delta\boldsymbol{\varphi}, \bar{\mathbf{t}} \rangle_{\Gamma_{\boldsymbol{\sigma}}} = 0 \quad \forall \delta\boldsymbol{\varphi} \ , \tag{37}$$

   or equivalently,

$$\langle \delta\boldsymbol{\varphi}, \rho_0 \mathbf{a}_{\mathrm{n}} \rangle_0 + \langle \mathrm{GRAD}_{\mathbf{X}}[\delta\boldsymbol{\varphi}], \mathbf{P}_{\mathrm{n}} \rangle_0 - \langle \delta\boldsymbol{\varphi}, \rho_0 \mathbf{b} \rangle_0 - \left\langle \delta\boldsymbol{\varphi}, \bar{\mathbf{T}} \right\rangle_{\bar{\Gamma}_{\boldsymbol{\sigma}}} = 0 \quad \forall \delta\boldsymbol{\varphi} \ . \tag{38}$$

2. Modify the accelerations for contact:

   (a) Predict the velocity field:

$$\mathbf{v}_{\mathrm{n}+1/2}^{\mathrm{pred}} = \mathbf{v}_{\mathrm{n}-1/2} + \bar{\mathrm{h}} \mathbf{a}_{\mathrm{n}} \ . \tag{39}$$

   (b) Predict the displacement field(s):

$$\mathbf{u}_{\mathrm{n}+1}^{\mathrm{pred}} = \mathrm{h}_{\mathrm{n}+1} \mathbf{v}_{\mathrm{n}+1/2}^{\mathrm{pred}} \ , \tag{40}$$

$$\mathsf{U}_{\mathrm{n}+1}^{\mathrm{pred}} = \mathsf{U}_{\mathrm{n}} + \mathbf{u}_{\mathrm{n}+1}^{\mathrm{pred}} \ . \tag{41}$$

   (c) Solve for the contact-induced accelerations: Compute a contact force based on gap-function calculations. The contact force affects the accelerations in that

$$\langle \delta\boldsymbol{\varphi}, \rho_{\mathrm{n}} \mathbf{a}_c \rangle_{\mathrm{n}} + \langle \delta\boldsymbol{\varphi}, \mathbf{t}_c \rangle_{\Gamma_c} = 0 \quad \forall \delta\boldsymbol{\varphi} \ , \tag{42}$$

   where $\mathbf{a}_c$ is the contact-inducted acceleration and $\mathbf{t}_c$ is the contact traction on $\Gamma_c \subseteq \Gamma \setminus (\Gamma_{\mathbf{u}} \bigcup \Gamma_{\boldsymbol{\sigma}})$.

(d) Correct the acceleration field: The computed accelerations are modified such that

$$\mathbf{a}_{\mathrm{n}} \mathrel{+}= \mathbf{a}_c \ . \tag{43}$$

3. Update the velocity field:

$$\mathbf{v}_{\mathrm{n}+1/2} = \mathbf{v}_{\mathrm{n}-1/2} + \bar{\mathrm{h}}\mathbf{a}_{\mathrm{n}} \tag{44}$$

4. Correct the computed velocity field to account for Dirichlet boundary conditions. This essentially involves resetting the values of $\mathbf{v}_{\mathrm{n}+1/2}$ to correspond to known data on any Dirichlet boundaries $\Gamma_{\mathbf{u}}$.

5. Compute the displacement field(s):

$$\mathbf{u}_{\mathrm{n}+1} = \mathrm{h}_{\mathrm{n}+1}\mathbf{v}_{\mathrm{n}+1/2}, \tag{45}$$

and/or set $\mathbf{u}_{\mathrm{n}+1}$ directly if the displacement is known on any Dirichlet boundaries $\Gamma_{\mathbf{u}}$. Then simply compute

$$\left.\begin{aligned} \mathbf{U}_{\mathrm{n}+1} &= \mathbf{U}_{\mathrm{n}} + \mathbf{u}_{\mathrm{n}+1} \\ \boldsymbol{\varphi}_{\mathrm{n}+1} &= \boldsymbol{\varphi}_{\mathrm{n}} + \mathbf{u}_{\mathrm{n}+1} \end{aligned}\right\} \ . \tag{46}$$

6. Calculate the incremental work done and update the internal energy $\varepsilon_{\mathrm{n}+1}$ of each material (see Section 5).

7. Given the (corrected) displacement field(s), compute the deformation $\mathbf{F}_{\mathrm{n}+1}$ and compute the stress $\boldsymbol{\sigma}_{\mathrm{n}+1}$. This step is discussed in Section 6.

8. Data swap: $\{\mathbf{U}_{\mathrm{n}}, \mathbf{v}_{\mathrm{n}-1/2}, \boldsymbol{\sigma}_{\mathrm{n}}, \varepsilon_{\mathrm{n}}\} \Longleftarrow\!\!\!\Longrightarrow \{\mathbf{U}_{\mathrm{n}+1}, \mathbf{v}_{\mathrm{n}+1/2}, \boldsymbol{\sigma}_{\mathrm{n}+1}, \varepsilon_{\mathrm{n}+1}\}$. Goto one(1).

(End **Algorithm Central-Difference**) ♦

Remarks 3.1.

1. Step one(1) is only correct assuming the use of a "lumped" mass matrix. If the mass matrix is "consistent" step one(1) must be modified. Let $\bar{\mathbf{a}}_{\mathrm{n}} : \Omega_{\mathrm{n}} \longmapsto \mathbb{R}^3$ be an acceleration field such that $\bar{\mathbf{a}}_{\mathrm{n}}(\mathbf{x})$ is known if $\mathbf{x}$ is on a Dirichlet boundary $\Gamma_{\mathbf{u}}$. (It is entirely possible that $\bar{\mathbf{a}}_{\mathrm{n}} = \mathbf{0}$.) Assume the virtual displacement field $\delta\boldsymbol{\varphi}$ is "admissible" in the sense that $\delta\boldsymbol{\varphi} = \mathbf{0}$ on any Dirichlet boundary $\Gamma_{\mathbf{u}}$. In step one(1) solve

$$\langle \delta\boldsymbol{\varphi}, \rho_{\mathrm{n}} \left(\bar{\mathbf{a}}_{\mathrm{n}} + \tilde{\mathbf{a}}_{\mathrm{n}}\right)\rangle_{\mathrm{n}} + \left\langle \mathrm{grad}_{\mathrm{n}}^{(s)}\, \delta\boldsymbol{\varphi}, \boldsymbol{\sigma}_{\mathrm{n}} \right\rangle_{\mathrm{n}} - \langle \delta\boldsymbol{\varphi}, \rho\mathbf{b}\rangle_{\mathrm{n}} - \langle \delta\boldsymbol{\varphi}, \bar{\mathbf{t}}\rangle_{\Gamma_\sigma} = 0 \quad \forall \delta\boldsymbol{\varphi} \ ,$$

where $\tilde{\mathbf{a}}_{\mathrm{n}} : \Omega_{\mathrm{n}} \longmapsto \mathbb{R}^3$ is zero on all Dirichlet boundaries $\Gamma_{\mathbf{u}}$. The total acceleration is then $\mathbf{a}_n = \bar{\mathbf{a}}_n + \tilde{\mathbf{a}}_{\mathrm{n}}$. This modification essentially decomposes the acceleration field into two components, one known and one unknown. In step four(4), the velocity correction must be algorithmically consistent with $\bar{\mathbf{a}}_{\mathrm{n}}$ on Dirichlet boundaries. Note that this of no particular concern since ALEGRA does in fact use only lumped mass matrices in the solid dynamics algorithms.

2. For frictionless contact, an augmented Lagrangian [42] node-on-surface contact algorithm is used. The details are omitted here, but the reader may consult [5, 17, 18, 50] for more information. For simulations without contact step two(2) may be omitted.

3. For purely mechanical problems the central difference algorithm is second-order accurate in time.

4. Notice that the velocities are explicitly computed at times $\mathrm{t}_{\mathrm{n}-1/2}$ and $\mathrm{t}_{\mathrm{n}+1/2}$. If the velocity at time t_{n} is needed, it is evaluated as

$$\mathbf{v}_{\mathrm{n}} := \frac{1}{2}\left(\mathbf{v}_{\mathrm{n}-1/2} + \mathbf{v}_{\mathrm{n}+1/2}\right) \ . \tag{47}$$

5. In many references [56, 60, 69], the central-difference method is written as[1]

$$\left.\begin{aligned} \langle \delta\boldsymbol{\varphi}, \rho_{\mathrm{n}}\mathbf{a}_{\mathrm{n}}\rangle_{\mathrm{n}} + \left\langle \mathrm{grad}_{\mathrm{n}}^{(s)}\, \delta\boldsymbol{\varphi}, \boldsymbol{\sigma}_{\mathrm{n}} \right\rangle_{\mathrm{n}} &= 0 \quad \forall \delta\boldsymbol{\varphi} \\ \mathbf{U}_{\mathrm{n}+1} = \mathbf{U}_{\mathrm{n}} + \mathrm{h}\mathbf{v}_{\mathrm{n}} + \frac{1}{2}\mathrm{h}^2\mathbf{a}_{\mathrm{n}} \\ \mathbf{v}_{\mathrm{n}+1} = \mathbf{v}_{\mathrm{n}} + \frac{1}{2}\mathrm{h}(\mathbf{a}_{\mathrm{n}} + \mathbf{a}_{\mathrm{n}+1}) \end{aligned}\right\} \ , \tag{48}$$

[1] For convenience, body forces and applied tractions are omitted.

for a time step $h > 0$. This is equivalent to the form presented in Algorithm Central-Difference, at least for a constant time step $h := h_n = h_{n+1} = \bar{h}$. First, rewrite equation $(48)_3$ as

$$h^2 \mathbf{a}_n = 2h(\mathbf{v}_{n+1} - \mathbf{v}_n) - h^2 \mathbf{a}_{n+1} \ . \tag{49}$$

The substitution of this into equation $(48)_2$ produces

$$\mathbf{U}_{n+1} - \mathbf{U}_n = h\mathbf{v}_{n+1} - \frac{1}{2} h^2 \mathbf{a}_{n+1} \ . \tag{50}$$

The time step index (n) is arbitrary here and thus

$$\mathbf{U}_n - \mathbf{U}_{n-1} = h\mathbf{v}_n - \frac{1}{2} h^2 \mathbf{a}_n \ . \tag{51}$$

The subtraction of equation (51) from equation $(48)_2$ yields

$$\mathbf{U}_{n+1} - 2\mathbf{U}_n + \mathbf{U}_{n-1} = h^2 \mathbf{a}_n \ . \tag{52}$$

However, equations (44) - (46) imply

$$\left.\begin{aligned} h^2 \mathbf{a}_n &= h(\mathbf{v}_{n+1/2} - \mathbf{v}_{n-1/2}) \\ &= (\mathbf{U}_{n+1} - \mathbf{U}_n) - (\mathbf{U}_n - \mathbf{U}_{n-1}) \\ &= \mathbf{U}_{n+1} - 2\mathbf{U}_n + \mathbf{U}_{n-1} \end{aligned}\right\} \ , \tag{53}$$

which is the desired result. Both representations produce the same displacement difference stencil. This demonstrates the equivalence of the two alternative representations of the central-difference method.

Remarks 3.2.

1. Many of the material models in ALEGRA require an approximation of the velocity gradient $\mathbf{l} = \mathbf{d} + \mathbf{w}$ to perform constitutive updates and compute the stress. In ALEGRA these approximations are

$$\mathbf{l}_{n+1/2} = \text{grad}_{n+1/2}[\mathbf{v}_{n+1/2}] \ , \tag{54}$$

$$\mathbf{d}_{n+1/2} = \text{symm}[\mathbf{l}_{n+1/2}] \ , \tag{55}$$

and

$$\mathbf{w}_{n+1/2} = \text{skew}[\mathbf{l}_{n+1/2}] \ . \tag{56}$$

2. Notice that

$$\begin{aligned} h_{n+1}\mathbf{l}_{n+1/2} &= \text{grad}_{n+1/2}[\tilde{\mathbf{u}}_{n+1}] \\ &= \text{grad}_n[\mathbf{u}_{n+1}]\, \mathbf{f}_{n+1/2}^{-1} \\ &= \text{grad}_n[(\boldsymbol{\varphi}_{n+1} - \boldsymbol{\varphi}_n) \circ \boldsymbol{\varphi}_n^{-1}]\, \mathbf{f}_{n+1/2}^{-1} \\ &= (\mathbf{f}_{n+1} - \mathbf{I})\, \mathbf{f}_{n+1/2}^{-1} \\ &= 2(\mathbf{f}_{n+1} - \mathbf{I})(\mathbf{f}_{n+1} + \mathbf{I})^{-1} \ . \end{aligned}$$

3. Under a superposed rigid body motion (SRBM), $\boldsymbol{\varphi}_{n+1} = \mathbf{Q}\boldsymbol{\varphi}_n$ for some $\mathbf{Q} \in SO(3)$. In this circumstance, $\mathbf{d}_{n+1/2} = \mathbf{0}$. To see this, notice that in this situation $\mathbf{f}_{n+1} = \mathbf{Q}$,

$$\mathbf{f}_{n+1/2} = \frac{1}{2}(\mathbf{I} + \mathbf{Q}),$$

and thus

$$h_{n+1}\mathbf{l}_{n+1/2} = 2(\mathbf{Q} - \mathbf{I})(\mathbf{Q} + \mathbf{I})^{-1}.$$

The reader may easily verify that

$$\text{symm}\left[(\mathbf{Q} + \mathbf{I})^T \mathbf{l}_{n+1/2}(\mathbf{Q} + \mathbf{I})\right] = \mathbf{0}.$$

Thus $\mathbf{l}_{n+1/2}$ is skew. (See also Corollary 8.1 of [96].)

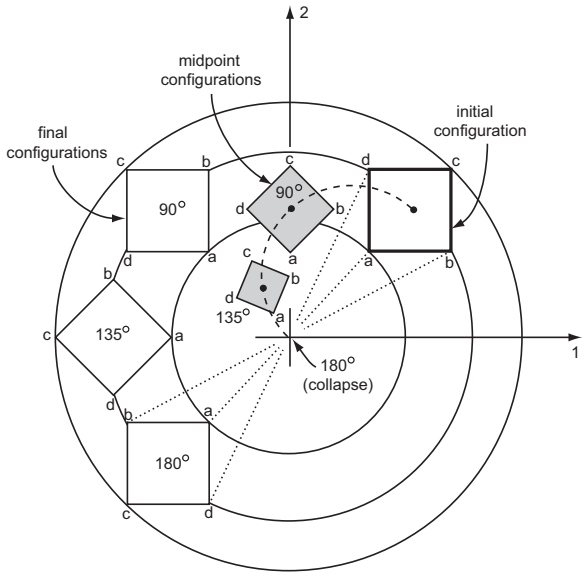

Figure 3. Behavior of the average(midpoint) configuration as a function of rotation. This figure is similar to figure one(1) of reference [57].

4. The immediately preceding analysis ensuring incremental objectivity of $\mathbf{l}_{n+1/2}$ requires that $(\mathbf{Q}+\mathbf{I})$ be non-singular. This is equivalent to requiring that -1 not be an eigenvalue of $\mathbf{Q}$. In that pathological case $\mathbf{Q}$ represents a rotation of π radians and the "average configuration" collapses to a point; see figure 3. Thus the algorithm for computing $\mathbf{l}$ is restricted to rotation increments strictly less than π radians. Fortunately, such a large rotation increment is generally beyond the range of expected values for an explicit time-stepping algorithm like the central-difference method. More details can be found in [57].

5. There are multiple possibilities for computing the polar decomposition $\mathbf{F}_{n+1/2} = \mathbf{V}_{n+1/2}\mathbf{R}_{n+1/2}$. Clearly, one way is the "DG" method; just compute them directly [51, 52]. Another way is the "VR" method as suggested by Dienes [35, 39, 62]. The Dienes algorithm is described in excellent detail by reference [41], which includes a flowchart outlining its implementation in an explicit time-stepping scheme. In either case, it is now assumed that $\mathbf{V}_{n+1/2}$ and $\mathbf{R}_{n+1/2}$ are available for use.

4 Spatial Approximation

In almost all regards ALEGRA uses a standard finite element spatial interpolations. Uniform strain isoparametric tensor product elements transformed from the parent domain $[-1,1]^{N_{\text{dim}}}$ are used [7, 8, 40]. These correspond to four-node quadrilateral elements in two dimensions are eight-node hexahedral elements in three dimensions. These are the simplest (non-locking) elements available for general purpose finite element analysis. Standard nodal shape functions are used to interpolate continuous fields such as position, velocity and acceleration. Shape function gradients are calculated by appropriate transformation of natural coordinate gradients [56, 112]. Any needed kinematic tensor fields are computed using the shape function gradients.

For standard finite element analysis,

$$\boldsymbol{\varphi} = \sum_{A=0}^{N_{\text{nodes}}-1} N^A \boldsymbol{\varphi}_A \implies \text{grad}[\boldsymbol{\varphi}] = \sum_{A=0}^{N_{\text{nodes}}-1} \boldsymbol{\varphi}_A \otimes \text{grad}[N^A] \,, \tag{57}$$

where $\boldsymbol{\varphi}_A$ is the value of $\boldsymbol{\varphi}$ at node A and the shape function for node A is denoted by N^A. The same spatial

interpolation is applied to $\delta\boldsymbol{\varphi}$. Thus equation (37) can be written for node A in matrix form as

$$\sum_{B=0}^{N_{\text{nodes}}-1} M^{AB}\mathbf{a}_B + \mathbf{F}^A_{\text{int}} - \mathbf{F}^A_{\text{ext}} \;=\; \mathbf{0}, \tag{58}$$

where

$$M^{AB} = \int_{\Omega_{\text{n}}} \rho_{\text{n}} N^A N^B \,\mathrm{d}\Omega_{\text{n}} \;, \tag{59}$$

is the mass matrix,

$$\mathbf{F}^A_{\text{int}} := \int_{\Omega_{\text{n}}} \boldsymbol{\sigma}_{\text{n}} \,\text{grad}_{\text{n}}[N^A] \,\mathrm{d}\Omega_{\text{n}} \;, \tag{60}$$

is the internal force vector at node A and

$$\mathbf{F}^A_{\text{ext}} := \int_{\Omega_{\text{n}}} N^A \rho_{\text{n}} \mathbf{b}_{\text{n}} \,\mathrm{d}\Omega_{\text{n}} \;+\; \int_{\Gamma_{\text{n}}} N^A \bar{\mathbf{t}} \,\mathrm{d}\Gamma_{\text{n}} \;, \tag{61}$$

is the external force vector at node A. If the mass matrix is lumped then

$$\bar{M}^A := \sum_{B=0}^{N_{\text{nodes}}-1} \left[\int_{\Omega_{\text{n}}} \rho_{\text{n}} N^A N^B \,\mathrm{d}\Omega_{\text{n}}\right] \;=\; \left[\int_{\Omega_{\text{n}}} \rho_{\text{n}} N^A \,\mathrm{d}\Omega_{\text{n}}\right] \;,$$

and $M^{AB} = \bar{M}^A \delta^{AB}$ (no sum on A).

All force integrals in ALEGRA are evaluated using a "mean quadrature" approach [40]. For example, equation (60) is numerically evaluated using the approximation

$$\mathbf{F}^A_{\text{int}} \approx \bar{\boldsymbol{\sigma}}_{\text{n}} \int_{\Omega_{\text{n}}} \text{grad}_{\text{n}}[N^A] \,\mathrm{d}\Omega_{\text{n}} \;,$$

where $\bar{\boldsymbol{\sigma}}$ is the (spatially constant) stress in the element. This stress is calculated using the mean volumetric deformation, the mean deformation gradient and/or the mean rate of deformation tensor for the element. The mean value of a kinematic field $(\cdot)$ in an element Ω_e is calculated as

$$\bar{(\cdot)} := \frac{1}{\text{meas}(\Omega_e)} \int_{\Omega_e} (\cdot) \,\mathrm{d}\Omega_e \;. \tag{62}$$

All relevant (thermodynamic) fields, which include but are not limited to, deformation rate, stress, pressure, density and internal energy, are assumed spatially constant in each element. Thus position and velocity are $C^0(\Omega) \subset H^1(\Omega)$ fields defined by nodal values and thermodynamic quantities are $L^2(\Omega)$ fields defined by piecewise constant element values. This is often referred to as a *staggered grid* spatial interpolation [23, 25]. Note also that a given kinematic field can be non-zero pointwise but may still have a zero mean value. In particular, there exist deformation modes for four-node planar and eight-node brick elements which have zero mean deformation. To avoid propagation of these zero-energy spurious modes hourglass control (section 8) is required.

Remarks 4.1. Using the divergence theorem, some volume integrals can be converted to surface integrals. For example,

$$\int_{\Omega} \text{grad}[N^A] \,\mathrm{d}\Omega \;=\; \int_{\Gamma} N^A \mathbf{n} \,\mathrm{d}\Gamma \;,$$

where Γ is the boundary of Ω and $\mathbf{n}$ is the outward normal. This approach to integral evaluation can reduce the total number of floating point computations, especially for elements such as the four-node quadrilateral, which has straight sides.

5 Energy Calculations

Step six(6) of algorithm central-difference requires a computation of the updated internal energy for each material. This section discusses the method ALEGRA uses for this update.

5.1 Existing ALEGRA Algorithm

Assuming no external heat sources and *adiabatic* conditions, equation (25) reduces to

$$\rho_{\mathrm{t}}\dot{\varepsilon} = (\boldsymbol{\sigma}_{\mathrm{t}} \bullet \mathbf{d}_{\mathrm{t}}) \; . \tag{63}$$

One simple way to integrate this numerically is the generalized midpoint rule

$$\rho_{\mathrm{n}+\beta} \cdot (\varepsilon_{\mathrm{n}+1} - \varepsilon_{\mathrm{n}}) = \bar{\mathrm{h}}(\boldsymbol{\sigma}_{\mathrm{n}+\beta} \bullet \mathbf{d}_{\mathrm{n}+\beta}) \quad \text{for} \quad \beta \in [0,1] \; . \tag{64}$$

Remarks 5.1.

1. Example material models.
   - Ideal gas.
     $$\boldsymbol{\sigma} = -(\gamma - 1)\rho_{\mathrm{t}}\varepsilon\mathbf{I} \; ,$$
     where $\gamma > 1$ is the ratio of the specific heats.
   - Viscous fluid.
     $$\boldsymbol{\sigma} = 2\mu \operatorname{dev} \mathbf{d}_{\mathrm{t}} \; ,$$
     where $\mu > 0$ is the dynamic shear viscosity.
   - Hyper-elasticity. See section 6.2.
2. For an element e with domain $\Omega_e \subseteq \Omega_{\mathrm{t}}$,
   $$\begin{aligned}
   \langle \boldsymbol{\sigma}_{\mathrm{t}}, \mathbf{d}_{\mathrm{t}} \rangle_{\mathrm{t}} &= \langle \boldsymbol{\sigma}_{\mathrm{t}}, \mathbf{l}_{\mathrm{t}} \rangle_{\mathrm{t}} \\
   &= \left\langle \boldsymbol{\sigma}_{\mathrm{t}}, \sum_{A=0}^{N_{\mathrm{nodes}}-1} \mathbf{v}_A \otimes \operatorname{grad}[N^A] \right\rangle_{\mathrm{t}} \\
   &= \sum_{A=0}^{N_{\mathrm{nodes}}-1} \left\langle \mathbf{v}_A, \boldsymbol{\sigma}_{\mathrm{t}} \operatorname{grad}[N^A] \right\rangle_{\mathrm{t}} \\
   &= \sum_{A=0}^{N_{\mathrm{nodes}}-1} \mathbf{v}_A \bullet \left[\int_{\Omega_e} \boldsymbol{\sigma}_{\mathrm{t}} \operatorname{grad}[N^A] \, \mathrm{d}\Omega_e \right] \\
   &= \sum_{A=0}^{N_{\mathrm{nodes}}-1} \mathbf{F}^A_{\mathrm{int}} \bullet \mathbf{v}_A
   \end{aligned}$$
3. The method above is implicit for $\beta > 0$. ALEGRA currently uses $\beta = 0$. Actually, what ALEGRA really does (for each element) is
   $$\left.\begin{aligned}
   \varepsilon_{\mathrm{n}+1} &= \varepsilon_{\mathrm{n}} \; + \; \bar{\mathrm{h}} \left[\int_{\Omega_{\mathrm{n}}} \rho_{\mathrm{n}} \, \mathrm{d}\Omega_{\mathrm{n}} \right]^{-1} \langle \boldsymbol{\sigma}_{\mathrm{n}}, \mathbf{d}_{\mathrm{n}} \rangle_{\mathrm{n}} \\
   &= \varepsilon_{\mathrm{n}} \; + \; \bar{\mathrm{h}} \left[\int_{\Omega_{\mathrm{n}}} \rho_{\mathrm{n}} \, \mathrm{d}\Omega_{\mathrm{n}} \right]^{-1} \left[\sum_{A=0}^{N_{\mathrm{nodes}}-1} \mathbf{F}^A_{\mathrm{int}} \bullet \mathbf{v}_A \right]_{\mathrm{n}} \\
   &= \varepsilon_{\mathrm{n}} \; + \; \bar{\mathrm{h}} M_e^{-1} \left[\sum_{A=0}^{N_{\mathrm{nodes}}-1} \mathbf{F}^A_{\mathrm{int}} \bullet \mathbf{v}_A \right]_{\mathrm{n}}
   \end{aligned}\right\} \; .$$
   The total mass of an element e is denoted by M_e. (Recall that all stress/strain/energy/density fields are constant within each cell.) The stress power is computed in `UnsDynamics::Calculate_Work()` and the energy is updated in `UnsDynamics::Update_Density_and_Energy()`. Notice that for $\beta = 0$ this is an *explicit* energy update, and does not depend on the state of the material at time $\mathrm{t}_{\mathrm{n}+1}$, only the state at time t_{n}.
4. Given that ALEGRA uses $\beta = 0$, *the algorithm, as implemented*, is only *first-order accurate*. Only the choice $\beta = 1/2$ is second-order accurate.

5.2 Equation(s) of State

For this class of materials assume the stress is simply $\boldsymbol{\sigma} = -\mathrm{p}\mathbf{I}$, where p is the (thermodynamic) pressure. Consistent with fluid dynamics convention the pressure is assumed positive in compression. Assume there exists an *equation of state* such that

$$\mathrm{p} = \hat{\mathrm{p}}(\rho, \varepsilon) \implies \boldsymbol{\sigma} = -\hat{\mathrm{p}}\mathbf{I}\,, \tag{65}$$

for a (smooth) function $\hat{\mathrm{p}} : \mathbb{R}^+ \times \mathbb{R}^+ \longmapsto \mathbb{R}$. For this class of materials, assuming the internal energy density $\varepsilon_{\mathrm{n}+\beta}$ (see section 5.1) and the density $\rho_{\mathrm{n}+\beta}$ have been computed, the pressure may be updated by a function evaluation

$$\mathrm{p}_{\mathrm{n}+\beta} = \hat{\mathrm{p}}(\rho_{\mathrm{n}+\beta}, \varepsilon_{\mathrm{n}+\beta}) \quad \forall \beta \in [0,1]\,. \tag{66}$$

The update of more complex material models is discussed in Section 6.

Remarks 5.2.

1. The density update is purely kinematic:

   $$\rho_{\mathrm{n}+\beta} = \det(\mathbf{f}_{\mathrm{n}+\beta})^{-1}\,\rho_{\mathrm{n}} \quad \forall \beta \in [0,1]\,.$$

   The density is updated in `UnsDynamics::Update_Density_and_Energy()`.

2. It may be possible to couple equations (65) - (66) with equation (64) for $\beta > 0$. This creates a (generally) *implicit coupled* system of equations for the pressure and the energy. The equations are non-linear and must be solved in some simultaneous iterative fashion [21]. With $\beta = 0$ the equations are uncoupled. Again, ALEGRA currently uses $\beta = 0$.

3. See `Ideal_Gas::Update_State(...)`. In this function it is assumed that $\varepsilon_{\mathrm{n}+1}$ has already been determined. Thus only the pressure is computed. All equation of state models in ALEGRA are implemented in this fashion (energy first, pressure second; an explicit, staggered, de-coupled update). See remark $(5.1)_3$.

4. All ALEGRA material model "updates" (hypo-elastic, hyper-elastic, equation of state, ideal gas...) are driven by `UnsEnergetics::Material_State_Update()`. This function is called *after* density and energy have been updated.

5. The reader may find it helpful to review the ALEGRA equations (for an ideal gas) in one(1) space dimension using a finite difference rather than a finite element notation. The one-dimensional stencils can be used for stability analysis, if desired, and are given in Appendix C.

5.3 Conservation Properties

The goal of this section is to discuss the global conservation properties of the ALEGRA algorithm. Only the case $\beta = 0$ is considered.

5.3.1 Angular Momentum

In absence of external tractions and body forces, the ALEGRA algorithm can be written in Lagrangian weak form as

$$\left\langle \delta\boldsymbol{\varphi}, \rho_0(\mathbf{v}_{\mathrm{n}+1/2} - \mathbf{v}_{\mathrm{n}-1/2})\right\rangle_0 \;+\; \bar{\mathrm{h}}\,\langle \mathrm{GRAD}_{\mathbf{X}}[\delta\boldsymbol{\varphi}], \mathbf{F}_{\mathrm{n}}\mathbf{S}_{\mathrm{n}}\rangle_0 \;=\; 0 \quad \forall\, \delta\boldsymbol{\varphi}. \tag{67}$$

Under suitable (pure Neumann) boundary conditions, an admissible choice for $\delta\boldsymbol{\varphi}$ is $\delta\boldsymbol{\varphi} = \mathbf{w} \times \boldsymbol{\varphi}_{\mathrm{n}}$ for some $\mathbf{w} \in \mathbb{R}^3$. A simple substitution yields

$$\left\langle \mathbf{w} \times \boldsymbol{\varphi}_{\mathrm{n}}, \rho_0(\mathbf{v}_{\mathrm{n}+1/2} - \mathbf{v}_{\mathrm{n}-1/2})\right\rangle_0 \;+\; \bar{\mathrm{h}}\,\langle \mathrm{GRAD}_{\mathbf{X}}[\mathbf{w} \times \boldsymbol{\varphi}_{\mathrm{n}}], \mathbf{F}_{\mathrm{n}}\mathbf{S}_{\mathrm{n}}\rangle_0 \;=\; 0\,. \tag{68}$$

Given any vector $\mathbf{w} \in \mathbb{R}^3$, there exists a unique 3×3 skew-symmetric tensor $\widehat{\mathbf{w}}$ such that $\mathbf{w} \times \mathbf{a} = \widehat{\mathbf{w}}\mathbf{a}\ \forall \mathbf{a} \in \mathbb{R}^3$. Using this property, the above equation can be written as

$$\left\langle \mathbf{w} \times \boldsymbol{\varphi}_{\mathrm{n}}, \rho_0(\mathbf{v}_{\mathrm{n}+1/2} - \mathbf{v}_{\mathrm{n}-1/2}) \right\rangle_0 \ + \ \bar{\mathrm{h}} \left\langle \mathrm{GRAD}_{\mathbf{X}}[\widehat{\mathbf{w}}\boldsymbol{\varphi}_{\mathrm{n}}], \mathbf{F}_{\mathrm{n}}\mathbf{S}_{\mathrm{n}} \right\rangle_0 \ = \ 0 \ . \tag{69}$$

Consider the second term on the left hand side:

$$\left.\begin{aligned} \left\langle \mathrm{GRAD}_{\mathbf{X}}[\widehat{\mathbf{w}}\boldsymbol{\varphi}_{\mathrm{n}}], \mathbf{F}_{\mathrm{n}}\mathbf{S}_{\mathrm{n}} \right\rangle_0 &= \left\langle \widehat{\mathbf{w}}\mathbf{F}_{\mathrm{n}}, \mathbf{F}_{\mathrm{n}}\mathbf{S}_{\mathrm{n}} \right\rangle_0 \\ &= \left\langle \widehat{\mathbf{w}}, \mathbf{F}_{\mathrm{n}}\mathbf{S}_{\mathrm{n}}\mathbf{F}_{\mathrm{n}}^T, \right\rangle_0 \\ &= 0 \end{aligned}\right\} \tag{70}$$

since the tensor $\mathbf{F}\mathbf{S}\mathbf{F}^T$ is symmetric and $\widehat{\mathbf{w}}$ is skew. This leaves only the first term, which by manipulating the cross product can be written as

$$\left\langle \mathbf{w}, \boldsymbol{\varphi}_{\mathrm{n}} \times \rho_0(\mathbf{v}_{\mathrm{n}+1/2} - \mathbf{v}_{\mathrm{n}-1/2}) \right\rangle_0 \ = 0 \ . \tag{71}$$

Since the vector $\mathbf{w}$ is arbitrary, this yields the conservation statement

$$\boxed{\int_{\Omega_0} \boldsymbol{\varphi}_{\mathrm{n}} \times \rho_0(\mathbf{v}_{\mathrm{n}+1/2} - \mathbf{v}_{\mathrm{n}-1/2}) \, \mathrm{d}\Omega_0 \ = \ \int_{\Omega_{\mathrm{n}}} \boldsymbol{\varphi}_{\mathrm{n}} \times \rho_{\mathrm{n}}(\mathbf{v}_{\mathrm{n}+1/2} - \mathbf{v}_{\mathrm{n}-1/2}) \, \mathrm{d}\Omega_{\mathrm{n}} \ = \ \mathbf{0} \, .} \tag{72}$$

Remarks 5.3. This conservation statement may seem somewhat odd to the reader. However, it is not inconsistent with the variational structure of the central difference method [60]. The variational structure of a time integration scheme guarantees that some momentum-like quantity (a momentum map [72]) is conserved [60, 69]. The conserved quantity is not necessarily intuitive or obvious, but is rather the consequence of a discrete version of Noether's Theorem [4].

5.3.2 Energy

Definition 5.1. The *total kinetic energy* is defined as

$$\mathsf{T}_{\mathrm{n}+\alpha} = \frac{1}{2} \int_{\Omega_0} \rho_0 \|\mathbf{v}_{\mathrm{n}+\alpha}\|^2 \, \mathrm{d}\Omega_0. \tag{73}$$

Definition 5.2. The *total internal energy* is defined as

$$\mathsf{V}_{\mathrm{n}+\alpha} = \int_{\Omega_0} \rho_0 \varepsilon_{\mathrm{n}+\alpha} \, \mathrm{d}\Omega_0. \tag{74}$$

In absence of external tractions and body forces, the ALEGRA algorithm can be written in Lagrangian weak form as

$$\left\langle \delta\boldsymbol{\varphi}, \rho_0(\mathbf{v}_{\mathrm{n}+1/2} - \mathbf{v}_{\mathrm{n}-1/2}) \right\rangle_0 \ + \ \bar{\mathrm{h}} \left\langle \mathrm{GRAD}_{\mathbf{X}}[\delta\boldsymbol{\varphi}], \mathbf{P}_{\mathrm{n}} \right\rangle_0 \ = \ 0 \quad \forall \, \delta\boldsymbol{\varphi}, \tag{75a}$$

$$\left\langle \zeta, \rho_0(\varepsilon_{\mathrm{n}+1} - \varepsilon_{\mathrm{n}}) \right\rangle_0 \ - \ \bar{\mathrm{h}} \langle \zeta, \mathbf{P}_{\mathrm{n}} \bullet \mathrm{GRAD}_{\mathbf{X}}[\mathbf{v}_{\mathrm{n}}] \rangle_0 \ = \ 0 \quad \forall \, \zeta, \tag{75b}$$

with

$$\mathbf{v}_{\mathrm{n}} := \frac{1}{2}(\mathbf{v}_{\mathrm{n}-1/2} + \mathbf{v}_{\mathrm{n}+1/2}) \, . \tag{76}$$

Under suitable (pure Neumann) boundary conditions, an admissible choice for $\delta\boldsymbol{\varphi}$ is $\delta\boldsymbol{\varphi} = \mathbf{v}_{\mathrm{n}}$. An admissible choice for ζ is $\zeta = 1$. With these substitutions, the above equations become

$$\mathsf{T}_{\mathrm{n}+1/2} - \mathsf{T}_{\mathrm{n}-1/2} + \Delta\mathsf{W} = 0, \tag{77a}$$

$$\mathsf{V}_{\mathrm{n}+1} - \mathsf{V}_{\mathrm{n}} - \Delta\mathsf{W} = 0, \tag{77b}$$

with the incremental work done defined as

$$\Delta\mathsf{W} \ := \ \bar{\mathrm{h}} \int_{\Omega_0} \mathbf{P}_{\mathrm{n}} \bullet \mathrm{GRAD}_{\mathbf{X}}[\mathbf{v}_{\mathrm{n}}] \, \mathrm{d}\Omega_0 \, . \tag{78}$$

Clearly this yields the total energy conservation statement

$$\boxed{\left(\mathsf{T}_{\mathrm{n}+1/2} + \mathsf{V}_{\mathrm{n}+1}\right) \quad - \quad \left(\mathsf{T}_{\mathrm{n}-1/2} + \mathsf{V}_{\mathrm{n}}\right) \ = \ 0.} \tag{79}$$

Remarks 5.4.

1. Numerical simulations using ALEGRA have suggested that the central difference method is mildly unstable for rapid adiabatic (isentropic) expansion(s) of ideal gases [29, 85]. Please see the continuing remarks which immediately follow and also Appendix D.
2. Notice that the energy update equation uses the time step $\bar{\mathrm{h}}$ rather than $\mathrm{h}_{\mathrm{n}+1}$. This is necessary to ensure that a statement of total energy conservation exists. However, the use of the time step $\bar{\mathrm{h}}$ does seem to be inconsistent with the time-centering of the internal energy.
3. One might argue that the above conservation statement is somewhat disconcerting. Notice that the time-centering of the kinetic energy is shifted by a half-step from the time centering of the internal energy. This does not imply that the conservation statement is invalid or incorrect. Nevertheless, it does bring into question the validity of the central difference method for strongly coupled thermo-mechanical continuum problems.
4. The central difference method is a very commonly used time integrator for continuum and structural dynamics. For purely mechanical problems the algorithmic properties are well understood and the method continues to be reliable and effective. However, for strongly coupled thermodynamic problems, the stability and conservation properties of the algorithm can be brought into question. These issues arise only for thermally (energetically) coupled problems, and not for the purely mechanical case [29, 85].
5. The reason that the choice $\beta = 1/2$ is not studied here is because the use of $\beta \neq 0$ generally leads to a non-conservative algorithm. The lack of a conserved energy *may* result in incorrect shock speeds (and thus shock locations) and a loss of convergence (to weak solutions) for hydrodynamic simulations (see paper [63] and book [101], section 9.6). Convergence to incorrect solutions is also possible [54].
6. An alternative second-order accurate energy update algorithm is proposed in Appendix A. Unfortunately, a conserved total energy quantity does not generally exist for that approach. More significantly, *the current* ALEGRA *central-difference based algorithm cannot in general achieve linear stability, global second-order accuracy and conservation of total energy simultaneously* [85].

5.3.3 Incremental Objectivity

The goal here is to determine the incremental objectivity properties of the ALEGRA energy update.

Proposition 5.1. Assume $\boldsymbol{\varphi}_{\mathrm{n}} = \mathbf{Q}_1\boldsymbol{\varphi}_{\mathrm{n}-1}$ and $\boldsymbol{\varphi}_{\mathrm{n}+1} = \mathbf{Q}_2\boldsymbol{\varphi}_{\mathrm{n}}$ for some $\mathbf{Q}_1, \mathbf{Q}_2 \in SO(3)$. Then the energy update is incrementally objective if $\mathrm{h}_{\mathrm{n}} = \mathrm{h}_{\mathrm{n}+1}$ and $\mathbf{Q}_1 = \mathbf{Q}_2$.

Proof. Using the update equations of section 3.2,

$$\left.\begin{aligned} \boldsymbol{\varphi}_{\mathrm{n}} &= \boldsymbol{\varphi}_{\mathrm{n}-1} + \mathrm{h}_{\mathrm{n}}\mathbf{v}_{\mathrm{n}-1/2} \\ \boldsymbol{\varphi}_{\mathrm{n}+1} &= \boldsymbol{\varphi}_{\mathrm{n}} + \mathrm{h}_{\mathrm{n}+1}\mathbf{v}_{\mathrm{n}+1/2} \end{aligned}\right\} , \tag{80}$$

under the kinematic assumptions of the proposition gives

$$\left.\begin{aligned} \mathbf{v}_{\mathrm{n}-1/2} &= \mathrm{h}_{\mathrm{n}}^{-1}(\boldsymbol{\varphi}_{\mathrm{n}} - \boldsymbol{\varphi}_{\mathrm{n}-1}) = \mathrm{h}_{\mathrm{n}}^{-1}(\mathbf{I} - \mathbf{Q}_1)\boldsymbol{\varphi}_{\mathrm{n}-1} = \mathrm{h}_{\mathrm{n}}^{-1}(\mathbf{I} - \mathbf{Q}_1)\mathbf{Q}_1^T\boldsymbol{\varphi}_{\mathrm{n}} = \mathrm{h}_{\mathrm{n}}^{-1}(\mathbf{Q}_1^T - \mathbf{I})\boldsymbol{\varphi}_{\mathrm{n}} \\ \mathbf{v}_{\mathrm{n}+1/2} &= \mathrm{h}_{\mathrm{n}+1}^{-1}(\boldsymbol{\varphi}_{\mathrm{n}+1} - \boldsymbol{\varphi}_{\mathrm{n}}) = \mathrm{h}_{\mathrm{n}+1}^{-1}(\mathbf{I} - \mathbf{Q}_2)\boldsymbol{\varphi}_{\mathrm{n}} \\ \mathbf{v}_{\mathrm{n}} &= \frac{1}{2}(\mathbf{v}_{\mathrm{n}-1/2} + \mathbf{v}_{\mathrm{n}+1/2}) = \frac{1}{2}\left[\mathrm{h}_{\mathrm{n}}^{-1}(\mathbf{Q}_1^T - \mathbf{I}) + \mathrm{h}_{\mathrm{n}+1}^{-1}(\mathbf{I} - \mathbf{Q}_2)\right]\boldsymbol{\varphi}_{\mathrm{n}} \end{aligned}\right\} . \tag{81}$$

Taking the material gradient of the velocity at time t_{n} results in

$$\mathrm{GRAD}_{\mathbf{X}}[\mathbf{v}_{\mathrm{n}}] = \frac{1}{2}\left[\mathrm{h}_{\mathrm{n}}^{-1}(\mathbf{Q}_1^T - \mathbf{I}) + \mathrm{h}_{\mathrm{n}+1}^{-1}(\mathbf{I} - \mathbf{Q}_2)\right]\mathbf{F}_n \, . \tag{82}$$

Now recall the incremental work done (78)

$$\Delta \mathsf{W} \;:=\; \bar{\mathrm{h}} \int_{\Omega_0} \mathbf{P}_{\mathrm{n}} \bullet \mathrm{GRAD}_{\mathbf{X}}[\mathbf{v}_{\mathrm{n}}] \, \mathrm{d}\Omega_0 \;\; = \;\; \bar{\mathrm{h}} \int_{\Omega_0} \mathbf{S}_{\mathrm{n}} \bullet \mathbf{F}_{\mathrm{n}}^T \, \mathrm{GRAD}_{\mathbf{X}}[\mathbf{v}_{\mathrm{n}}] \, \mathrm{d}\Omega_0 \, . \tag{83}$$

Since $\mathbf{S}$ is symmetric, a sufficient condition for $\Delta \mathsf{W} = 0$ is that $\mathbf{F}_{\mathrm{n}}^T \, \mathrm{GRAD}_{\mathbf{X}}[\mathbf{v}_{\mathrm{n}}]$ be skew. This is satisfied if and only if the quantity

$$\mathrm{h}_{\mathrm{n}}^{-1}(\mathbf{Q}_1^T - \mathbf{I}) + \mathrm{h}_{\mathrm{n+1}}^{-1}(\mathbf{I} - \mathbf{Q}_2) \; ,$$

is skew. This is satisfied in general only when $\mathrm{h}_{\mathrm{n}} = \mathrm{h}_{\mathrm{n+1}}$ and $\mathbf{Q}_1 = \mathbf{Q}_2$. □

Remarks 5.5.

1. The energy update is guaranteed incrementally objective only when $\mathrm{h}_{\mathrm{n}} = \mathrm{h}_{\mathrm{n+1}}$ and $\mathbf{Q}_1 = \mathbf{Q}_2$. Unfortunately, these are rather restrictive requirements and in general the energy update is *not objective*. In particular, a rigid body motion which occurs in a single time step does not generally produce zero incremental work done.

2. Incremental objectivity is not required for consistency, stability or convergence. However, it is a desirable property. Consider a continuum body rotating rigidly. If the energy update is not incrementally objective the internal energy of the material will change as the body rotates. Consequently, for an equation of state model the thermodynamic pressure will also change. The result in this case is spurious pressure variations when the pressure should remain constant in time.

Remarks 5.6.

1. Notice that time centering of the data $\mathbf{Z} := \{\mathbf{v}, \mathbf{x}, \boldsymbol{\sigma}, \varepsilon\}$ is staggered in a "leap-frog" fashion for the central-difference method. The velocity $\mathbf{v}$ and momentum are time located at the mid-points of a time interval, while the position $\mathbf{x}$ and energy ε are located at the end-points of a time interval. This makes the definition of algorithmic quantities such as total energy and total momentum somewhat difficult.

2. The resolution of the energy consistency issues discussed in this report may necessitate the use of an entirely different conservative time integration algorithm. A mid-point based predictor multi-corrector integrator has shown promise in this regard [93, 94]. That algorithm conserves total angular momentum and an algorithmically consistent and well defined total energy, and is incrementally objective in both stress and energy updates.

3. All data for the mid-point time integrator is centered at the end-points of a time interval. The integrator is implicitly a map from $\mathbf{Z}_{\mathrm{n}} \mapsto \mathbf{Z}_{\mathrm{n+1}}$. In fact, the algorithm can be written abstractly as

   $$\mathbf{Z}_{\mathrm{n+1}} = \mathbf{Z}_{\mathrm{n}} \; + \; \mathrm{h}_{\mathrm{n+1}} \cdot \mathbb{F}(\mathbf{Z}_{\mathrm{n+1/2}}, \mathrm{h}_{\mathrm{n+1}}) \; ,$$

   for an appropriately defined function $\mathbb{F}$. Algorithmic quantities such as total energy and total momentum are easily defined. The details are in references [93, 94].

6 Stress Update Algorithm

Step seven(7) of algorithm central-difference requires a computation of the updated stress response of the material. The method for performing the constitutive update depends upon the type of material being used.

6.1 Hypo-Elasticity

The concept of hypo-elasticity was originally introduced by Truesdell [103]. More details can be found in [11, 98, 104]. Assume a constitutive model of the form

$$\dot{\boldsymbol{\Sigma}}_{\mathrm{t}} = \mathbb{C}\mathbf{D}_{\mathrm{t}} \; , \tag{84}$$

where the rank-four tensor $\mathbb{C}$ is positive-definite (coercive) in the sense that

$$\exists \, \kappa > 0 \text{ such that } \forall \, \mathbf{v}, \mathbf{w} \in \mathbb{R}^3 \quad (\mathbf{v} \otimes \mathbf{w}) \bullet \mathbb{C} \, (\mathbf{v} \otimes \mathbf{w}) \geqslant \kappa \|\mathbf{v}\|^2 \|\mathbf{w}\|^2 \; . \tag{85}$$

Let $\beta \in [0, 1]$. The algorithm is as follows [96]:

1. Compute the material rate of deformation:

$$\mathbf{D}_{\mathrm{n}+\beta} = \mathbf{R}_{\mathrm{n}+\beta}^T \mathbf{d}_{\mathrm{n}+\beta} \mathbf{R}_{\mathrm{n}+\beta}$$

2. Compute the material stress:

$$\boldsymbol{\Sigma}_n = \mathbf{R}_n^T \boldsymbol{\sigma}_n \mathbf{R}_n$$

3. Update the material stress:

$$\boldsymbol{\Sigma}_{\mathrm{n}+1} = \boldsymbol{\Sigma}_n + \mathrm{h}_{\mathrm{n}+1} \mathbb{C} \mathbf{D}_{\mathrm{n}+\beta}$$

4. Rotate forward to get Cauchy stress:

$$\boldsymbol{\sigma}_{\mathrm{n}+1} = \mathbf{R}_{\mathrm{n}+1} \boldsymbol{\Sigma}_{\mathrm{n}+1} \mathbf{R}_{\mathrm{n}+1}^T$$

Remarks 6.1.

1. Assume that $\mathbf{d}_{\mathrm{n}+\beta}$ is incrementally objective. Then the algorithm above is incrementally objective. Given the way ALEGRA computes the rate of deformation tensor, only the choice $\beta = 1/2$ is incrementally objective.

2. Even with the choice $\beta = 1/2$, under a SRBM $\mathbf{f}_{\mathrm{n}+1} = \mathbf{Q} \in SO(3)$, the Cauchy stresses will transform exactly as $\boldsymbol{\sigma}_{\mathrm{n}+1} = \mathbf{Q} \boldsymbol{\sigma}_n \mathbf{Q}^T$ if and only if $\mathbf{R}_{\mathrm{n}+1} \mathbf{R}_{\mathrm{n}}^T = \mathbf{Q}$. The Dienes algorithm [35, 41, 62] only approximates this condition and does not exactly reproduce $\mathbf{Q}$ as the incremental rotation.

3. Residual stresses may remain at the end of a closed strain path for hypo-elastic materials [61, 90].

4. General models of *hypo*-elasticity are *incompatible with* the notion of *hyper*-elasticity [11, 98, 104]. More precisely, given a hypo-elastic material model, there does not generally exist a corresponding Helmholtz free energy function for that model. Thus the model lacks a solid mathematical basis relative to rational thermodynamics [1, 30, 31, 102] and quantities such as internal energy and heat production are ill-defined. The extension of this class of material models to the full thermo-elastic regime remains unclear.

5. Hypo-elastic models remain in common use in many commercial and government computational software applications [49, 62]. However, most if not all academic researchers in computational mechanics have long since abandoned hypo-elasticity in favor of thermodynamically consistent models of material behavior.

6. The use of a hypo-elastic material model does *not* guarantee that the continuum evolution equations define an (infinite-dimensional) Hamiltonian system. A Lagrangian action integral is not well defined and as such the variational structure of the central-difference method is undetermined in this case.

6.2 Hyper-Elasticity

Given the thermodynamic issues associated with hypo-elasticity, one might want to consider alternative models of material behavior. From a rigorous thermodynamic perspective, hyper-elasticity is more correct; hypo-elasticity has proven useful, but remains problematic thermodynamically. For a comprehensive overview of continuum thermodynamics the reader may consult [34, 71, 104].

Let $\Theta > 0$ be the absolute temperature field. Given a Helmholtz free energy density $\Psi(\mathbf{C}, \Theta)$ (per unit mass) [1, 30, 31, 71, 104]

$$\mathbf{S}_{\mathrm{n}+\alpha} = 2\rho_0 \left[\frac{\partial \Psi}{\partial \mathbf{C}} \right]_{\{\mathbf{C},\Theta\} = \{\mathbf{C}_{\mathrm{n}+\alpha}, \Theta_{\mathrm{n}+\alpha}\}} . \tag{86}$$

Then simply

$$\boldsymbol{\sigma}_{\mathrm{n}+\alpha} = J_{\mathrm{n}+\alpha}^{-1} \mathbf{F}_{\mathrm{n}+\alpha} \mathbf{S}_{\mathrm{n}+\alpha} \mathbf{F}_{\mathrm{n}+\alpha}^T . \tag{87}$$

This holds $\forall \alpha \in [0, 1]$.

Remarks 6.2.

1. There is essentially no need for objective stress rates relative to hyper-elasticity. The material model is purely "strain-driven," and stresses can be computed and updated directly from the total deformation $\mathbf{F}_{n+1}$ (or the incremental deformation $\mathbf{f}_{n+1}$) and the time step $h_{n+1} > 0$. This is true even with visco-elastic, visco-plastic and damage extensions.

2. The use of a hyper-elastic material model (under the assumption of constant temperature, or alternatively constant entropy [104]) ensures that the continuum evolution equations define an (infinite-dimensional) Hamiltonian system. In this situation, the central-difference method is a *variational* time integrator [60, 69]. The time-discrete equations of the method can be derived as the Euler-Lagrange equations of a time-discrete Lagrangian action integral. Subject to time step restrictions, the method possesses rather remarkable stability and conservation properties.

3. Thermo-Elasticity [1, 2, 32, 46, 71, 76, 97]:

   Internal Entropy Density (per unit mass) :

$$\eta = -\partial_\Theta \Psi(\mathbf{C}, \Theta) \tag{88}$$

   Internal Energy Density (per unit mass) :

$$\varepsilon = \hat{\varepsilon}(\mathbf{C}, \Theta) \;=\; \Psi(\mathbf{C}, \Theta) + \eta(\mathbf{C}, \Theta) \cdot \Theta \; . \tag{89}$$

   ThermoElastic Heating:

$$\mathcal{H} = -\frac{1}{2}\Theta \cdot \partial_\Theta(\mathbf{S} \bullet \dot{\mathbf{C}}) = -\Theta \cdot \Big[\rho_0(\partial_{\Theta\mathbf{C}}\Psi) \bullet \dot{\mathbf{C}}\Big] \tag{90}$$

   Specific Heat (per unit mass):

$$c := -\Theta \cdot \partial^2_{\Theta\Theta}\Psi \tag{91}$$

   Heat Conduction:

   (a) Entropy form:

$$\rho_0 \Theta \dot{\eta} = [-J \operatorname{div} \mathbf{q} + \rho_0 \mathcal{R}] \tag{92}$$

   (b) Temperature form:

$$\rho_0 c \dot{\Theta} = -\mathcal{H} \;+\; [-J \operatorname{div} \mathbf{q} + \rho_0 \mathcal{R}], \tag{93}$$

   where $\mathbf{q}$ is the spatial (Cauchy) heat flux and $\mathcal{R}$ is the external heat source per unit mass. In general the specific heat $c > 0$ is *not* constant.

4. Note that an equation-of-state model may be considered a special case of thermo-elasticity. Once the updated density and internal energy are calculated, the (thermodynamic) pressure is computed by a function evaluation (see Section 5.2). More abstractly, for an equation-of-state model the free energy is assumed to be function of volume and temperature $\Psi(\det \mathbf{C}, \Theta)$.

5. Ideal gas. Consistent with the immediately preceding remark, an ideal gas is in fact a type of thermo-elastic material. The internal energy of an ideal gas is given by

$$\varepsilon(\rho, \eta) = \varepsilon_0 \left[\frac{\rho}{\rho_0} \exp\left(\frac{\eta - \eta_0}{R}\right)\right]^{(\gamma-1)} , \tag{94}$$

   where $R > 0$ is the gas constant, $\gamma > 1$ is the adiabatic exponent and $\{\rho_0, \eta_0, \varepsilon_0\}$ is the reference state of the gas [77]. A standard sequence of thermodynamic arguments yields (see chapter 2 of [33])

$$p = \rho^2 \partial_\rho \varepsilon \implies p = (\gamma - 1)\rho\epsilon \; ,$$

   and

$$\Theta = \partial_\eta \varepsilon \implies \Theta = c_{\mathrm{v}}^{-1} \varepsilon \; ,$$

where $c_{\mathrm{v}} = (\gamma - 1)^{-1} R$ is the constant volume specific heat capacity per unit mass. This equation may be inverted in closed form as

$$\eta - \eta_0 = R \log \left[\frac{\rho_0}{\rho} \left(\frac{c_{\mathrm{v}} \Theta}{\varepsilon_0} \right)^{\frac{1}{\gamma - 1}} \right] , \tag{95}$$

and thus

$$\Psi(\rho, \Theta) = \varepsilon \left(\rho, \eta(\rho, \Theta) \right) \; - \; \eta(\rho, \Theta) \cdot \Theta \; .$$

Note also that $\rho_0 / \rho = (\det \mathbf{C})^{1/2}$.

6. As another example, consider a volumetric-deviatoric uncoupled thermoelastic material. In this case, a simple form for the free energy is [97]

$$\Psi(\mathbf{C}, \Theta) = \underbrace{\hat{T}(\Theta) + \hat{M}(J, \Theta)}_{\text{thermal}} + \underbrace{\hat{W}(\tilde{\mathbf{C}}) + \hat{U}(J)}_{\text{elastic}} ,$$

where $\tilde{\mathbf{C}} := J^{-2/3} \mathbf{C}$. For a *neo-hookean* model, these functions may take the form

$$\left. \begin{aligned} \hat{T}(\Theta) &= c_0 \left[(\Theta - \Theta_0) - \Theta \log \left(\frac{\Theta}{\Theta_0} \right) \right] \\ \hat{M}(J, \Theta) &= -3\beta (\Theta - \Theta_0) \hat{U}'(J) \\ \hat{W}(\mathbf{C}) &= \frac{1}{2} \rho_0^{-1} \mu \left[\operatorname{trace}(\mathbf{C}) - 3 \right] \\ \hat{U}(J) &= \rho_0^{-1} \kappa \left[\frac{1}{2} (J^2 - 1) - \log(J) \right] \end{aligned} \right\} ,$$

where $\Theta_0 > 0$ is the reference temperature, $c_0 > 0$ is the reference heat capacity, $\beta > 0$ is the (linearized) coefficient of thermal expansion, $\kappa > 0$ is the (linearized) bulk modulus and $\mu > 0$ is the (linearized) shear modulus.

7. For *non-dissipative* materials, which include ideal gas and other equation of state models, the use of equation (63), ignoring heat fluxes and heat sources (and artificial viscosity), implies an *isentropic* process. For non-dissipative materials heat conduction

$$\gamma_{\mathrm{con}} := -\frac{1}{\rho \Theta^2} (\mathbf{q} \bullet \operatorname{grad} \Theta) \geqslant 0 ,$$

is the only source of local entropy production [30, 32, 34, 104]. For hyper-elasticity, see remark $(6.2)_8$.

8. For hyper-elastic materials assume that the internal energy density ε is a function of deformation and temperature (see [104], section 82),

$$\varepsilon = \hat{\varepsilon}(\mathbf{C}, \Theta) \; = \; \Psi(\mathbf{C}, \Theta) + \eta(\mathbf{C}, \Theta) \cdot \Theta \; ,$$

where Ψ is the (Helmholtz) free energy density and η is the specific entropy, both per unit mass. Then it should be possible, given $\varepsilon_{\mathrm{n}+1}$, to solve for $\Theta_{\mathrm{n}+1}$ implicitly by solving

$$\varepsilon_{\mathrm{n}+1} - \hat{\varepsilon}(\mathbf{C}_{\mathrm{n}+1}, \Theta_{\mathrm{n}+1}) = 0 \; .$$

This is equivalent to numerically approximating adiabatic (and thus isentropic) thermo-elasticity; see equation (92).

9. For general hypo-elastic (section 6.1) material models an internal energy function does not exist. A discussion of dissipation and/or entropy production is meaningless.

7 Shock Capturing

7.1 Background information

In shock physics calculations, physical viscosity[2] is truly negligible and has space and time scales much smaller than those resolved by the grid. The weak, or integral, Euler equations are inherently ill-posed (having an infinite number of solutions). Computational solutions involving shocks, without some form of stability control, usually have severe oscillations because of this. Mathematically, it is common practice to add a viscosity term to shock equations and consider the unique solution arising in the limit as the viscosity vanishes. This approach is known as viscosity solutions. Computationally, a similar effect can be achieved by use of an artificial viscosity to stabilize the computed solution about a shock [64].

Like physical viscosity, artificial viscosity appears in both the fluid momentum and energy equations through the stress tensor. In the momentum equation the artificial viscosity stress, $\boldsymbol{\sigma}_{\text{av}}$, should act to reduce momentum at the shock front, and hence also reduce the kinetic energy there. In the energy equation, the kinetic energy lost should be dissipated (and entropy produced [32]) by raising the fluid internal energy ($\boldsymbol{\sigma}_{\text{av}} \bullet \mathbf{d} \geqslant 0$). Thus, like physical viscosity, artificial viscosity acts to convert kinetic energy into internal energy at the shock front. To form an artificial viscosity stress tensor, one must construct artificial analogs of physical terms such as $\mu \propto \rho v_{\text{th}} \lambda$ and $\mathbf{d}$.

7.2 Standard Artificial Viscosity

The basic von Neumann-Richtmyer artificial viscosity [106] idea is to exchange the space and time scales from the physical viscosity for ones applicable to the grid and fluid velocity. They replaced the term $v_{\text{th}}\lambda$ in μ with the product of a term proportional to the spatial gradient of the velocity and a space-scale squared. The space-scale is selected to be a grid length, resulting in a compact smearing of the shock. This basic idea,

$$\boldsymbol{\sigma}_{\text{visc,quad}} = \left(\rho h^2 \|\mathbf{d}\|\right) \cdot \|\mathbf{d}\| \longleftarrow (\rho v_{\text{th}} \lambda) \, \|\mathbf{d}\| \, , \tag{96}$$

results in a term quadratic in the velocity gradient. In multidimensional applications, the simplest approach is to use a scalar coefficient and to compute $\|\mathbf{d}\|$ as trace[$\mathbf{d}$], independent of shock direction (since evaluating the shock direction robustly remains an open problem). This simplest application in multiple space dimensions is what ALEGRA uses for its quadratic term,

$$\boldsymbol{\sigma}_{\text{visc,quad,ALEGRA}} = \mathbf{Q}_{\text{quad}} = \left(\rho l^2 \, |\text{trace}[\mathbf{d}]|\right) \cdot \text{trace}[\mathbf{d}] \cdot \mathbf{I} \, , \tag{97}$$

where $l > 0$ is what NEVADA calls the aspect ratio (an element characteristic length scale).

This term is quadratic in $\mathbf{d}$, whereas the physical viscous stress is only linear in $\mathbf{d}$. The second $\mathbf{d}$ in the quadratic term really serves only to help define the space and time scales over which the artificial viscosity acts. An alternative is to use the sound speed $c_s > 0$ to obtain those space/time scales. This results in the linear term used in ALEGRA

$$\boldsymbol{\sigma}_{\text{visc,lin,ALEGRA}} = \mathbf{Q}_{\text{lin}} = (\rho l c_s) \, \text{trace}[\mathbf{d}] \cdot \mathbf{I} \, . \tag{98}$$

Thus the final form for the standard artificial viscosity used in ALEGRA is

$$\boxed{\boldsymbol{\sigma}_{\text{visc}} = \rho \left(\, c_1 l c_s \; + \; c_2 l^2 \, |\text{trace}[\mathbf{d}]| \, \right) \text{trace}[\mathbf{d}] \, \mathbf{I} \, ,} \tag{99}$$

where $c_1 > 0$ is the linear constant and $c_2 > 0$ is the quadratic constant. This is the general linear plus quadratic form most commonly used in shock hydrodynamics calculations [9, 22, 26, 37, 78, 108].

Remarks 7.1.

[2]The physical dynamic viscosity coefficient $\mu \propto \rho v_{\text{th}} \lambda$ is proportional to the product of the density, the thermal speed ($v_{\text{th}} \propto \sqrt{\Theta}$) and the molecular collision mean free path λ.

1. For the compressible Euler equations, the standard Galerkin finite element solution conserves total entropy [55]. Without an additional numerical entropy production mechanism, the standard Galerkin method cannot correctly capture shocks and will not converge to an entropy satisfying solution of the Euler equations in the presence of shocks.
2. Viscous stresses are a source of dissipation and entropy production [32, 104].
3. Based on the theory presented in [75], the artificial viscosity should be explicitly material dependent. Note that the linear term of equation (99) depends on the sound speed of the material, but unfortunately the quadratic term does not.

7.3 Calculation of the rate of deformation

In order to be consistent with the central-difference method, the artificial shock capturing viscous stresses should be computed at time t_{n+1}. This requires an approximation to $\mathbf{d}_{n+1}$, which has not been previously discussed. The following definitions prove useful in this regard:

Definition 7.1. The *pull-back* [7] of a rank-two contravariant spatial tensor $\boldsymbol{\tau}$ is

$$\boldsymbol{\varphi}^*\boldsymbol{\tau} := \mathbf{F}^{-1}\boldsymbol{\tau}\,\mathbf{F}^{-T} . \tag{100}$$

The corresponding *push-forward* of a contravariant material tensor $\mathbf{S}$ is denoted by $\boldsymbol{\varphi}_*\mathbf{S}$.

Definition 7.2. The *pull-back* [7] of a rank-two covariant spatial tensor $\mathbf{g}$ is

$$\boldsymbol{\varphi}^*\mathbf{g} := \mathbf{F}^{T}\mathbf{g}\,\mathbf{F} . \tag{101}$$

The corresponding *push-forward* of a covariant material tensor $\mathbf{G}$ is denoted by $\boldsymbol{\varphi}_*\mathbf{G}$.

Definition 7.3. The *rate of deformation* tensor $\mathbf{d}$ is one-half the *Lie derivative* of the spatial metric $\mathbf{g}$ [7]. More precisely, $2\mathbf{d} = \mathcal{L}_{\mathbf{v}}[\mathbf{g}]$, where

$$\mathcal{L}_{\mathbf{v}}[\mathbf{g}] = \boldsymbol{\varphi}_*\left(\frac{\mathrm{d}}{\mathrm{dt}}\boldsymbol{\varphi}^*\mathbf{g}\right) . \tag{102}$$

Without any significant loss of generality, the spatial metric is henceforward assumed to be the identity $\mathbf{g} = \mathbf{I}$.

Given these definitions, the rate of deformation $\mathbf{d}$ my be computed as

$$\left.\begin{aligned} 2\mathbf{d} &= \mathcal{L}_{\mathbf{v}}[\,\mathbf{I}\,] \\ &= \mathbf{F}^{-T}\left[\frac{\mathrm{d}}{\mathrm{dt}}(\mathbf{F}^T\mathbf{I}\,\mathbf{F})\right]\mathbf{F}^{-1} \\ &= \mathbf{F}^{-T}\dot{\mathbf{C}}\mathbf{F}^{-1} \end{aligned}\right\} . \tag{103}$$

Inverting this equation yields

$$\left.\begin{aligned} \dot{\mathbf{C}} &= 2\mathbf{F}^T\mathbf{d}\mathbf{F} \\ &= 2\mathbf{F}^T\mathbf{d}\mathbf{F}^{-T}\mathbf{C} \\ &= 2\left[\mathbf{F}^T\mathbf{d}\mathbf{F}^{-T}\right]\mathbf{C} \end{aligned}\right\} . \tag{104}$$

A backward-Euler exponential approximation in time of equation (104) produces

$$\left.\begin{aligned} \mathbf{C}_{n+1} &\approx \exp\left[2h_{n+1}\mathbf{F}_{n+1}^T\mathbf{d}_{n+1}\mathbf{F}_{n+1}^{-T}\right]\mathbf{C}_n \\ &= \mathbf{F}_{n+1}^T\exp[2h_{n+1}\mathbf{d}_{n+1}]\,\mathbf{F}_{n+1}^{-T}\mathbf{C}_n \end{aligned}\right\} . \tag{105}$$

Inverting this equation yields

$$\left.\begin{aligned} \exp[2h_{n+1}\mathbf{d}_{n+1}] &= \mathbf{F}_{n+1}^{-T}\mathbf{C}_{n+1}\mathbf{C}_n^{-1}\mathbf{F}_{n+1}^T \\ &= \mathbf{F}_{n+1}^{-T}\mathbf{F}_{n+1}^T\mathbf{F}_{n+1}\mathbf{F}_n^{-1}\mathbf{F}_n^{-T}\mathbf{F}_{n+1}^T \\ &= (\mathbf{F}_{n+1}\mathbf{F}_n^{-1})(\mathbf{F}_{n+1}\mathbf{F}_n^{-1})^T \\ &= \mathbf{f}_{n+1}\mathbf{f}_{n+1}^T \end{aligned}\right\} . \tag{106}$$

The end result is

$$\mathbf{d}_{n+1} = \frac{1}{2h_{n+1}} \log[\mathbf{f}_{n+1}\mathbf{f}_{n+1}^T] \,. \tag{107}$$

Lemma 7.1. $\det[\exp \mathbf{A}] = \exp[\operatorname{trace} \mathbf{A}]$ for all $n \times n$ matrices $\mathbf{A}$.

Proof. First, assume $\mathbf{A}$ is diagonalizable. Then there exists an invertible matrix $\mathbf{S}$ and a diagonal matrix $\mathbf{D}$ such that $\mathbf{A} = \mathbf{S}\mathbf{D}\mathbf{S}^{-1}$. In this case, $\exp \mathbf{A} = \mathbf{S}[\exp \mathbf{D}]\mathbf{S}^{-1}$ and $\det[\exp \mathbf{A}] = \det[\exp \mathbf{D}]$. However, for a diagonal matrix this determinant is simply the product of the exponential of the eigenvalues λ_k

$$\begin{aligned}
\det[\exp \mathbf{A}] &= \det[\exp \mathbf{D}] \\
&= \prod_{k=0}^{n-1} \exp(\lambda_k) \\
&= \exp\left[\sum_{k=0}^{n-1} \lambda_k\right] \\
&= \exp[\operatorname{trace} \mathbf{D}] \\
&= \exp[\operatorname{trace} \mathbf{A}] \,.
\end{aligned}$$

The proof is completed by noting that diagonalizable matrices are a *dense* subset of all matrices. □

Proposition 7.2. The derived approximation for $\mathbf{d}_{n+1}$ is both incrementally objective and volume preserving.

Proof. Incremental objectivity is satisfied by construction. Alternatively, it follows from the fact that $\log \mathbf{I} = \mathbf{0}$. As for volume preservation,

$$\begin{aligned}
j_{n+1}^2 &= \det[\mathbf{f}_{n+1}\mathbf{f}_{n+1}^T] \\
&= \det(\exp[2h_{n+1}\mathbf{d}_{n+1}]) \\
&= \exp[2h_{n+1} \cdot \operatorname{trace} \mathbf{d}_{n+1}] \,.
\end{aligned}$$

Thus $j_{n+1} = 1$ if and only if $\operatorname{trace} \mathbf{d}_{n+1} = 0$. □

Remarks 7.2.

1. The ALEGRA shock capturing artificial viscosity can be turned on/off in tension ($\operatorname{trace}[\mathbf{d}] > 0$), if desired. The viscosity is always on in compression ($\operatorname{trace}[\mathbf{d}] < 0$).
2. See `PRONTO_Artificial_Viscosity::Update_Artificial_Viscosity(...)`.
3. The present default implementation of ALEGRA uses $\mathbf{d}_{n+1/2}$ rather than $\mathbf{d}_{n+1}$ to compute the artificial viscosity pressure. This may not be consistent with the central-difference method.
4. This logarithmic option my be turned on by typing `LOGARITHMIC = ON`.

7.4 Tensor Artificial Viscosity

A *tensor* artificial viscosity can help stabilize mesh deformation in some circumstances [22, 80, 91, 93]. Based on the results presented in [93], a tensor artificial viscosity may be computed as

$$\boldsymbol{\sigma}_{\text{visc}} := \rho\nu\mathbf{d}, \tag{108}$$

where $\nu > 0$ is the *kinematic* viscosity. The kinematic viscosity is computed as

$$\nu := c_1\, c_s\, l \;+\; c_2\, |\operatorname{trace}(\mathbf{d})|\, l^2, \tag{109}$$

where $c_1 > 0$ is the linear constant, $c_2 > 0$ is the quadratic constant, $l > 0$ is a mesh-based characteristic length scale and $c_s > 0$ is the sound speed of the material.

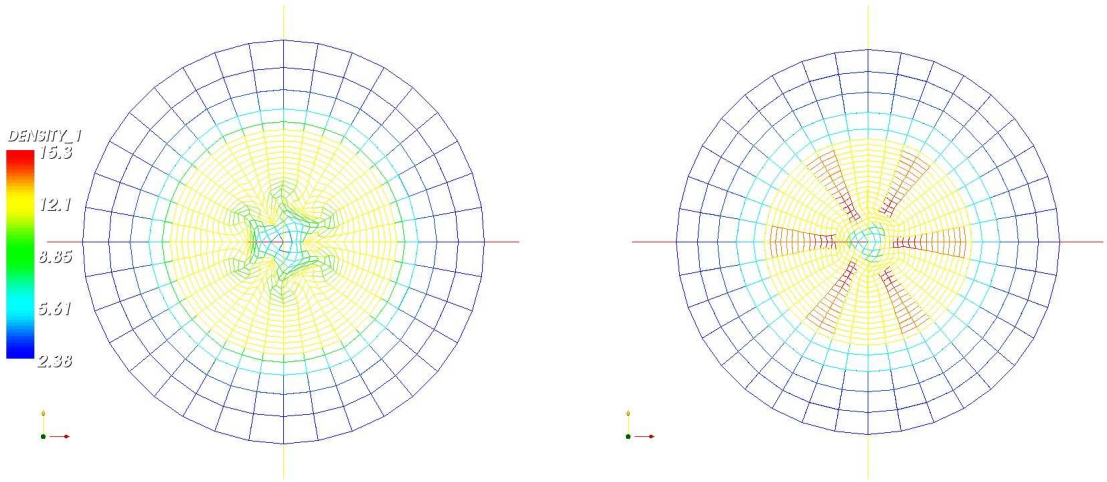

(a) Standard scalar artificial viscosity of equation (99)

(b) Tensor artificial viscosity of Section (7.4)

Figure 4. Noh test, gamma-law ideal gas, on radial trisection mesh [93]. Radially convergent initial velocity field. Deformed meshes colored by contours of density.

Remarks 7.3.

1. See figure (4) for example simulation results.
2. Notice that the tensor viscosity above is symmetric. Some researchers have considered non-symmetric artificial viscosities [9, 24] in an attempt to stabilize spurious vorticity [38]. Unfortunately, angular momentum is conserved in general if and only if the stress tensor is symmetric. In an effort not to disrupt angular momentum conservation, which the authors consider to be an important and fundamental property of the continuum system, only symmetric algorithmic stress tensors are considered in ALEGRA .
3. This option is invoked in the input file using the keyword `TENSOR ARTIFICIAL VISCOSITY`.

8 Hourglass Control

The goal of this section is to review the hourglass control algorithms currently implemented in ALEGRA .

8.1 Shape Function Representations

In what follows, attention is primarily focused upon the eight(8)-node isoparametric tri-linear brick element for which $N_{\text{nodes}} = 8$. Following the presentation(s) in [8] [82] [95], let $\mathbf{N}(\boldsymbol{\xi})$ denote the 8×1 vector of shape functions such that

$$\mathbf{N}(\boldsymbol{\xi}) = \{N^1, N^2, \ldots, N^8\}^T \quad \text{with} \quad N^A := \frac{1}{8}(1 + \xi_1\xi_1^A)(1 + \xi_2\xi_2^A)(1 + \xi_3\xi_3^A) \ , \tag{110}$$

where $\boldsymbol{\xi}^A = \{\xi_1^A, \xi_2^A, \xi_3^A\}^T$ are the vertices of the bi-unit cube $[-1, 1]^3$. These shape functions may be written as

$$\mathbf{N}(\boldsymbol{\xi}) = \mathbf{b}_0 + \sum_{i=1}^{3} x_i \mathbf{b}_i + \frac{1}{8}\sum_{j=1}^{4} \mathcal{H}_j(\boldsymbol{\xi})\boldsymbol{\gamma}_j \ , \tag{111}$$

where $\mathcal{H}_(\boldsymbol{\xi})$ are the *hourglass functions* defined as

$$\mathcal{H}_1(\boldsymbol{\xi}) := \xi_2\xi_3 \ , \quad \mathcal{H}_2(\boldsymbol{\xi}) := \xi_3\xi_1 \ , \quad \mathcal{H}_3(\boldsymbol{\xi}) := \xi_1\xi_2 \ , \quad \mathcal{H}_4(\boldsymbol{\xi}) := \xi_1\xi_2\xi_3 \ . \tag{112}$$

The twelve(12)-dimensional *hourglass deformation space* of the eight-node brick is defined as

$$\mathbb{H}_{12} := \text{span}\{\mathcal{H}_1, \mathcal{H}_2, \mathcal{H}_3, \mathcal{H}_4\} \times \mathbb{R}^3 \ . \tag{113}$$

This space may be viewed as consisting of four(4) *hourglass modes*, where each mode can act in any one of three(3) coordinate directions.

The constant 8×1 vectors $\mathbf{b}_0$, $\mathbf{b}_i$ and $\boldsymbol{\gamma}_j$ can be determined in a relatively straight-forward manner. Evaluation of equation (111) at the nodes of the bi-unit cube and use of the Kronecker property $N^A(\xi_B) = \delta_{AB}$ yields the 8×8 matrix expression

$$\mathbf{I}_8 = \mathbf{b}_0 \otimes \mathbf{1}_8 + \sum_{i=1}^{3} \mathbf{b}_i \otimes \mathbf{x}_i + \frac{1}{8} \sum_{j=1}^{4} \boldsymbol{\gamma}_j \otimes \mathbf{h}_j \ . \tag{114}$$

In this equation $\mathbf{I}_8$ is the 8×8 identity matrix, $\mathbf{x}_i = \{x_i^1, x_i^2, \ldots, x_i^8\}^T$ is the 8×1 vector of nodal coordinates for component i and

$$\left.\begin{aligned} \mathbf{1}_8 &:= \{1,1,1,1,1,1,1,1\}^T \\ \mathbf{h}_1 &:= \{1,1,-1,-1,-1,-1,1,1\}^T \\ \mathbf{h}_2 &:= \{1,-1,-1,1,-1,1,1,-1\}^T \\ \mathbf{h}_3 &:= \{1,-1,1,-1,1,-1,1,-1\}^T \\ \mathbf{h}_4 &:= \{-1,1,-1,1,1,-1,1,-1\}^T \end{aligned}\right\} \ . \tag{115}$$

The reader may easily verify that $\mathbf{1}_8 \bullet \mathbf{h}_j = 0$ and $\mathbf{h}_j \bullet \mathbf{h}_k = 8\delta_{jk}$. The multiplication of equation (114) by the vector $\mathbf{1}_8$ yields the equation

$$\mathbf{b}_0 = \frac{1}{8} \left[\mathbf{1}_8 - \sum_{i=1}^{3} (\mathbf{1}_8 \bullet \mathbf{x}_i) \mathbf{b}_i \right] \ . \tag{116}$$

The multiplication of equation (114) by the vector $\mathbf{h}_k$ yields the equation

$$\boldsymbol{\gamma}_j = \left[\mathbf{h}_j - \sum_{i=1}^{3} (\mathbf{h}_j \bullet \mathbf{x}_i) \mathbf{b}_i \right] \ . \tag{117}$$

Taking the derivative of (111) with respect to x_k (or, alternatively, ξ_k) and evaluation at the element center $\boldsymbol{\xi} = \mathbf{0}$ yields

$$\mathbf{b}_i = \sum_{j=1}^{3} \left(\mathbf{J}_0^{-T}\right)_{ij} \frac{\partial \mathbf{N}}{\partial \xi_j}(\mathbf{0}) \quad \text{where} \quad \mathbf{J}_0 := \frac{\partial \mathbf{x}}{\partial \boldsymbol{\xi}}(\mathbf{0}) \ . \tag{118}$$

Since $\mathbf{b}_i$ are consistently computed 'strain-displacement' operators, one can show that (see [56], chapter 3)

$$\mathbf{b}_i \bullet \mathbf{1}_8 = 0 \quad \text{and} \quad \mathbf{b}_i \bullet \mathbf{x}_j = \delta_{ij} \ . \tag{119}$$

Given these properties, it must also hold from (117) that

$$\boldsymbol{\gamma}_i \bullet \mathbf{1}_8 = 0 \quad \text{and} \quad \boldsymbol{\gamma}_i \bullet \mathbf{x}_j = 0 \ , \tag{120}$$

and thus the vectors $\boldsymbol{\gamma}_i$ *are orthogonal to the homogeneous deformation modes* of the tri-linear brick element. Finally,

note that in nodal components

$$\left.\begin{aligned}\gamma_j(A) &= h_j(A) \;-\; \sum_{i=1}^{3}(h_j \bullet \mathbf{x}_i)\mathbf{b}_i(A) \\ &= h_j(A) \;-\; \sum_{i=1}^{3}\left(\mathbf{b}_i(A) \;\cdot\; \sum_{B=1}^{N_{\text{nodes}}} h_j(B)x_i(B)\right) \\ &=: h_j(A) \;-\; \mathbf{b}_A \;\bullet\; \sum_{B=1}^{N_{\text{nodes}}} h_j(B)\mathbf{x}_B \\ &=: h_j(A) \;-\; \mathbf{b}_A \;\bullet \mathbf{y}_j\end{aligned}\right\}, \tag{121}$$

where

$$\mathbf{b}_A := \mathbf{J}_0^{-T}\,\text{GRAD}_{\boldsymbol{\xi}}[N^A(\mathbf{0})] \quad \text{and} \quad \mathbf{y}_j := \sum_{B=1}^{N_{\text{nodes}}} h_j(B)\mathbf{x}_B\;. \tag{122}$$

Remarks 8.1.

1. For a four node quadrilateral element there is only one(1) hourglass function $\mathcal{H}(\boldsymbol{\xi}) := \xi_1\xi_2$ and one(1) hourglass vector $\mathbf{h} = \{1, -1, 1, -1\}^T$. All the other developments above remain essentially unchanged. The details are omitted.

2. In actual numerical implementations of two(2)-dimensional problems in ALEGRA , the hourglass vector $\mathbf{h}$ is normalized so that $\|\mathbf{h}\| = 1$. In three(3)-dimensional simulations, this normalization is not performed and $\|\mathbf{h}_i\| = \sqrt{8}$.

8.2 Hourglass Rates

Let $\mathbf{v}^h(A)$ for $A \in \{1, 2, \ldots, N_{\text{nodes}}\}$ denote the nodal velocity field of a finite element. Consistent with the developments in [7] [8] [40] [107], define the *hourglass rate* for mode m as

$$\mathbf{r}_m^{hg} := \sum_{A=1}^{N_{\text{nodes}}} \gamma_m(A)\mathbf{v}^h(A)\;. \tag{123}$$

8.3 Hourglass Resistance

The goal here is to compute, based on the hourglass rates $\mathbf{r}_m^{hg}$, a reasonable value of the hourglass resistance $\mathbf{f}_m^{hg}$.

8.3.1 Pisces

Based on the work in [44], the hourglass resistance for an element e is computed as

$$\mathbf{f}_m^{hg} := \left[\left(2 - \frac{1}{2}N_{\text{dim}}\right) \cdot \nu_{hg} \cdot c_s \cdot \frac{\rho \cdot \text{meas}(\Omega_e)}{h_e}\right] \cdot \mathbf{r}_m^{hg}\;, \tag{124}$$

where $N_{\text{dim}} \geq 2$ is the number of spatial problem dimensions, $h_e > 0$ is an element characteristic length scale, $c_s > 0$ is the maximum material wave speed (ideally determined from an eigenvalue analysis of the acoustic tensor [104]) and $\nu_{hg} > 0$ is a user defined parameter.

8.3.2 Pronto

The Pronto [62] hourglass viscosity coefficient is given by

$$\mu_{hg} := \begin{cases} \nu_{hg} \cdot \sqrt{128.0 \cdot G \cdot \rho \cdot \text{meas}(\Omega_e)} & \text{if 2-D} \\ \nu_{hg} \cdot \sqrt{1.5 \cdot G \cdot \rho \cdot (\text{meas}(\Omega_e))^2 h_e^{-2}} & \text{if 3-D} \end{cases} , \tag{125}$$

where $G > 0$ is the (linearized) shear modulus of the material and $\nu_{hg} > 0$ is a user defined parameter. The Pronto hourglass control also has the option to time integrate the hourglass 'rate' to determine an hourglass "stiffness". The Pronto hourglass stiffness coefficient is given by

$$\kappa_{hg} := \begin{cases} \mathrm{k}_{hg} \cdot 0.5 \cdot G \cdot \text{meas}(\Omega_e) \cdot h_e^{-2} & \text{if 2-D} \\ \mathrm{k}_{hg} \cdot 0.125 \cdot G \cdot \text{meas}(\Omega_e) \cdot h_e^{-2} & \text{if 3-D} \end{cases} , \tag{126}$$

where $\mathrm{k}_{hg} > 0$ is a user defined parameter.

Definition 8.1. The pull-back of a spatial one-form (co-vector) $\boldsymbol{\omega}$ is defined as

$$\boldsymbol{\varphi}^* \boldsymbol{\omega} := \mathbf{F}^T \boldsymbol{\omega} , \tag{127}$$

with corresponding push-forward operation $\boldsymbol{\varphi}_* \boldsymbol{\omega}$ (see section 1.2 of [71]).

Definition 8.2. The Lie derivative of a spatial one-form $\boldsymbol{\omega}$ is defined as

$$\mathcal{L}_{\mathbf{v}}[\boldsymbol{\omega}] = \boldsymbol{\varphi}_* \left(\frac{\mathrm{d}}{\mathrm{dt}} \boldsymbol{\varphi}^* \boldsymbol{\omega} \right) . \tag{128}$$

Define a time-integrated "stiffness" parameter $\mathbf{s}_m^{hg}$ for mode m such that

$$\mathcal{L}_{\mathbf{v}} \left[\mathbf{s}_m^{hg} \right] = \mathbf{F}^{-T} \frac{\mathrm{d}}{\mathrm{dt}} \left(\mathbf{F}^T \mathbf{s}_m^{hg} \right) = \mathrm{k}_{hg} \mathbf{r}_m^{hg} . \tag{129}$$

A simple approximation in time yields

$$\left. \begin{aligned} \mathcal{L}_{\mathbf{v}} \left[\mathbf{s}_m^{hg} \right] &\approx \mathbf{F}_{\mathrm{n+1}}^{-T} \left[\mathbf{F}_{\mathrm{n+1}}^T \mathbf{s}_m^{hg}(\mathrm{t_{n+1}}) - \mathbf{F}_{\mathrm{n}}^T \mathbf{s}_m^{hg}(\mathrm{t_n}) \right] \mathrm{h}_{\mathrm{n+1}}^{-1} \\ &= \mathrm{h}_{\mathrm{n+1}}^{-1} \left[\mathbf{s}_m^{hg}(\mathrm{t_{n+1}}) - \mathbf{F}_{\mathrm{n+1}}^{-T} \mathbf{F}_{\mathrm{n}}^T \mathbf{s}_m^{hg}(\mathrm{t_n}) \right] \\ &= \mathrm{h}_{\mathrm{n+1}}^{-1} \left[\mathbf{s}_m^{hg}(\mathrm{t_{n+1}}) - \mathbf{f}_{\mathrm{n+1}}^{-T} \mathbf{s}_m^{hg}(\mathrm{t_n}) \right] \end{aligned} \right\} . \tag{130}$$

This results in the discrete update equation

$$\mathbf{s}_m^{hg}(\mathrm{t_{n+1}}) = \mathbf{f}_{\mathrm{n+1}}^{-T} \mathbf{s}_m^{hg}(\mathrm{t_n}) \ + \ \mathrm{h_{n+1}} \mathrm{k}_{hg} \mathbf{r}_m^{hg} . \tag{131}$$

Finally, the hourglass resistance is computed as

$$\mathbf{f}_m^{hg} := \mu_{hg} \mathbf{r}_m^{hg} \ + \ \mathbf{s}_m^{hg} . \tag{132}$$

Remarks 8.2.

1. Clearly the Pronto hourglass control cannot be used for a frictionless material, in particular for frictionless gases, since the shear modulus $G = 0$.

2. The Lie derivative is an objective rate and the Pronto stiffness update algorithm is by construction incrementally objective.

3. The Pronto stiffness algorithm is implicitly equivalent to using a hypo-elastic material model for hourglass stabilization. Consistent with that, residual hourglass forces may remain at the end of a closed strain path [58].

8.4 Hourglass Nodal Forces

Let $\mathbf{F}_m^{hg}(A)$ for $A \in \{1, 2, \ldots, N_{\text{nodes}}\}$ denote the nodal hourglass force field for mode m of a tri-linear brick element. Once the hourglass resistance has been determined, the nodal forces for hourglass mode m are simply computed as

$$\mathbf{F}_m^{hg}(A) = \gamma_m(A) \cdot \mathbf{f}_m^{hg} \ . \tag{133}$$

8.5 Proposed alternative algorithm

There may be an alternative, albeit more computationally expensive, hourglass control algorithm. For an element e with domain $\Omega_e \subseteq \Omega$, define the mean value of the rate of deformation tensor as

$$\bar{\mathbf{d}} \ := \ \frac{1}{\text{meas } \Omega_e} \int_{\Omega_e} \mathbf{d} \, \mathrm{d}\Omega_e \ , \tag{134}$$

and the fluctuation from this mean as

$$\tilde{\mathbf{d}} := \mathbf{d} - \bar{\mathbf{d}} \ . \tag{135}$$

For hourglass control purposes, an artificial viscous stress of the form

$$\boldsymbol{\sigma}_{hg} := \rho \nu \tilde{\mathbf{d}} \tag{136}$$

can be added to the physical (and shock capturing) stress. In this equation, $\nu > 0$ is a kinematic viscosity, which may be computed as

$$\nu = c_{hg} c_s \, h_e \ , \tag{137}$$

with $c_{hg} > 0$ an hourglass control parameter. The nodal forces (for node A) associated with this stabilization are computed as

$$\mathbf{F}^{hg}(A) := \int_{\Omega_e} \boldsymbol{\sigma}_{hg} \, \text{grad}[N^A] \, \mathrm{d}\Omega_e \, . \tag{138}$$

Remarks 8.3.

1. This hourglass control algorithm passes the patch test by construction. For a homogeneous deformation, $\tilde{\mathbf{d}} = \mathbf{0}$.
2. This algorithm requires *full quadrature* to stabilize hourglass modes. The non-homogeneous component $\tilde{\mathbf{d}}$ of the deformation must be sampled at multiple points, not just at the element center, to fully detect hourglass modes.
3. The scaling of the hourglass resistance in this approach is similar to that of the Pisces algorithm equation (124).
4. A variational multi-scale based hourglass control algorithm, similar in concept to the one proposed here, is discussed in [93, 94].

9 Closure

This report has presented the algorithmic details of the ALEGRA continuum hydrodynamics package. The package uses a Galerkin finite element spatial discretization and an explicit central-difference stepping method in time. The details of the algorithm have been presented, along with its strengths and weaknesses. Some suggestions for further improvements and modifications have also been included. It is hoped that this report can help code developers and physics analysts more easily understand and modify ALEGRA .

The development and refinement of ALEGRA is ongoing. Some suggestions for future research and development include, but are not limited to, the following:

- Implementation of a truly second-order, (linearly) stable, conservative predictor multi-corrector time-stepping algorithm.
- The use of a limiter with the full tensor artificial viscosity to detect isentropic compression and reduce the viscosity smoothly to zero(0) in the absence of shocks.
- Implementation and use of thermodynamically consistent hyperelastic-based solid models for plasticity and failure.
- The coupling of X-FEM (see [105] and references therein) to the existing Lagrangian scheme to enable a better treatment of multi-material problems.
- Investigation into alternative spatial discretizations for Lagrangian shock hydrodynamics, including continuous pressure SUPG-stabilized formulations [92] and H(div) finite elements [3, 6, 12, 14, 15, 86, 87]. H(div) formulations are not typically used for Lagrangian hydrodynamics, but recent research has shown promise in that regard [83, 88].

Acknowledgment: The authors wish to thank Dr. Allen C. Robinson and Dr. Randall M. Summers for their continuing support and encouragement. The authors thank Dr. Allen C. Robinson, Dr. William J. Rider and Dr. Joshua Robbins for reviewing initial drafts of the report. The authors also thank Dr. William J. Rider and Dr. Guglielmo Scovazzi for helpful discussions. Mr. Kyle Cochrane very kindly provided the numerical simulation of Appendix D.

References

[1] Stuart S. Antman. *Nonlinear problems of elasticity*, volume 107 of *Applied Mathematical Sciences*. Springer, New York, 2nd edition, 2005.

[2] F. Armero and J. C. Simo. A new unconditionally stable fractional step method for non-linear coupled thermomechanical problems. *International Journal for Numerical Methods in Engineering*, **35**(4):737–766, September 1992.

[3] Douglas N. Arnold, Daniele Boffi, and Richard S. Falk. Quadrilateral H(div) finite elements. *SIAM Journal on Numerical Analysis*, **42**(6):2429–2451, 2005.

[4] V. I. Arnold. *Mathematical Methods of Classical Mechanics*, volume 60 of *Graduate Texts in Mathematics*. Springer, New York, 2nd edition, 1989.

[5] S. W. Attaway, B. A. Hendrickson, S. J. Plimpton, D. R. Gardner, C. T. Vaughan, K. H. Brown, and M. W. Heinstein. A parallel contact detection algorithm for transient solid dynamics simulations using PRONTO3D. *Computational Mechanics*, **22**(2):143–159, August 1998.

[6] C. Bahriawati and C. Carstensen. Three matlab implementations of the lowest-order Raviart-Thomas MFEM with a posteriori error control. *Computational Methods in Applied Mathematics*, **5**(4):333–361, 2005.

[7] Ted Belytschko, Wing Kam Liu, and Brain Moran. *Nonlinear finite elements for continua and structures*. John Wiley and Sons, New York, 2000.

[8] Ted Belytschko, Jame Shau-Jen Ong, Wing Kam Liu, and James M. Kennedy. Hourglass control in linear and nonlinear problems. *Computer Methods in Applied Mechanics and Engineering*, **43**(3):251–276, May 1984.

[9] David J. Benson. A new two-dimensional flux-limited shock viscosity for impact calculations. *Computer Methods in Applied Mechanics and Engineering*, **93**(1):1991, December 1991.

[10] David J. Benson. Computational methods in lagrangian and eulerian hydrocodes. *Computer Methods in Applied Mechanics and Engineering*, **99**(2-3):235–394, September 1992.

[11] Barry Bernstein. Hypo-elasticity and elasticity. *Archive for Rational Mechanics and Analysis*, **6**(1):89 – 104, January 1960.

[12] Pavel B. Bochev, Jonathan J. Hu, Allen C. Robinson, and Raymond S. Tuminaro. Towards robust 3d Z-pinch simulations: discretization and fast solvers for magnetic diffusion in heterogeneous conductors. *Electronic Transactions on Numerical Analysis*, **15**:186–210, 2003.

[13] Javier Bonet and Richard D. Wood. *Nonlinear Continuum Mechanics for Finite Element Analysis*. Cambridge University Press, September 1997.

[14] Franco Brezzi and Michel Fortin. *Mixed and Hybrid Finite Element Methods*, volume 15 of *Springer Series in Computational Mathematics*. Springer-Verlag, New York, 1991.

[15] Franco Brezzi, Jim Douglas Jr., and L. D. Marini. Two families of mixed finite elements for second order elliptic problems. *Numerische Mathematik*, **47**(2):217–235, June 1985.

[16] Alexander N. Brooks and Thomas J.R. Hughes. Streamline upwind/petrov-galerkin formulations for convection dominated flows with particular emphasis on the incompressible navier-stokes equations. *Computer Methods in Applied Mechanics and Engineering*, **32**(1-3):199–259, September 1982.

[17] Kevin H. Brown, Michael W. Glass, Arne S. Gullerud, Martin W. Heinstein, Reese E. Jones, and Randall M. Summers. ACME : a parallel library of algorithms for contact in a multi-physics environment. In K. J. Bathe, editor, *Proceedings of the First MIT Conference on Computational Fluid and Solid Mechanics*, Computational Fluid and Solid Mechanics, Cambridge, Massachusetts, June 2001. Massachusetts Institute of Technology, Elsevier. Sandia Report SAND2001-0904A.

[18] Kevin H. Brown, Martin W. Heinstein, Reese E. Jones, and Thomas E. Voth. Explicit transient dynamics enforcement of frictional sliding contact in ACME. Technical Report SAND2003-2809P, Sandia National Laboratories, Albuquerque, NM, July 2003. Proposed for presentation at the 7th US National Congress on Computational Mechanics held July 27-31, 2003 in Albuquerque, NM.

[19] Thomas A. Brunner, Todd J. Urbatsch, Thomas M. Evans, and Nicholas A. Gentile. Comparison of four parallel algorithms for domain decomposed implicit monte carlo. *Journal of Computational Physics*, **212**(2):527–539, March 2006.

[20] K. G. Budge and J. S. Peery. RHALE: A MMALE shock physics code written in C++. *International Journal of Impact Engineering*, **14**(1-4):107–120, 1993.

[21] Richard L. Burden and J. Douglas Faires. *Numerical analysis*. Brooks/Cole, Pacific Grove, CA, 7th edition, 2001.

[22] J. C. Campbell and M. J. Shashkov. A tensor artificial viscosity using a mimetic finite difference algorithm. *Journal of Computational Physics*, **172**(2):739–765, September 2001.

[23] E. J. Caramana, D. E. Burton, M. J. Shashkov, and P. P. Whalen. The construction of compatible hydrodynamics algorithms utilizing conservation of total energy. *Journal of Computational Physics*, **146**(1):227–262, October 1998.

[24] E. J. Caramana and R. Loubere. "Curl-q": A vorticity damping artificial viscosity for essentially irrotational lagrangian hydrodynamics calculations. *Journal of Computational Physics*, **215**(2):385–391, July 2006.

[25] E. J. Caramana, C. L. Rousculp, and D. E. Burton. A compatible, energy and symmetry preserving lagrangian hydrodynamics algorithm in three-dimensional cartesian geometry. *Journal of Computational Physics*, **157**(1):89–119, January 2000.

[26] E. J. Caramana, M. J. Shashkov, and P. P. Whalen. Formulations of artificial viscosity for multi-dimensional shock wave computations. *Journal of Computational Physics*, **144**(1):70–97, July 1998.

[27] P. Chadwick. *Continuum Mechanics: Concise Theory and Problems*. Dover Publications, Mineola, NY, 2nd expanded edition, November 1999.

[28] Phillipe. G. Ciarlet. *Mathematical Elasticity, Vol I : Three-Dimensional Elasticity*, volume 20 of *Studies in Mathematics and Its Applications*. North Holland, Amsterdam, 1988.

[29] Kyle R. Cochrane and William J. Rider. Sandia National Laboratories, Albuquerque, NM, January 2007. private communication.

[30] Bernard D. Coleman and Morton E. Gurtin. Thermodynamics with internal state variables. *The Journal of Chemical Physics*, **47**(2):597–613, July 1967.

[31] Bernard D. Coleman and Victor J. Mizel. Existence of caloric equations of state in thermodynamics. *The Journal of Chemical Physics*, **40**(4):1116–1125, February 1964.

[32] Bernard D. Coleman and Walter Noll. The thermodynamics of elastic materials with heat conduction and viscosity. *Archive for Rational Mechanics and Analysis*, **13**(1):167–178, December 1963.

[33] Constantine M. Dafermos. *Hyperbolic Conservation Laws in Continuum Physics*, volume 325 of *Grundlehren der mathematischen Wissenschaft*. Springer-Verlag, Berlin, 2nd edition, 2005.

[34] Alfredo Bermudez de Castro. *Continuum Thermomechanics*, volume 37 of *Progress in Mathematical Physics*. Birkhauser Basel, Boston, 2005.

[35] J. K. Dienes. On the analysis of rotation and stress rate in deforming bodies. *Acta Mechanica*, **32**:217–232, 1979.

[36] Guy Dimonte, D. L. Youngs, A. Dimits, S. Weber, M. Marinak, S. Wunsch, C. Garasi, A. Robinson, M. J. Andrews, P. Ramaprabhu, A. C. Calder, B. Fryxell, J. Biello, L. Dursi, P. MacNeice, K. Olson, P. Ricker, R. Rosner, F. Timmes, H. Tufo, Y.-N. Young, and M. Zingale. A comparative study of the turbulent Rayleigh-Taylor instability using high-resolution three-dimensional numerical simulations: The alpha-group collaboration. *Physics of Fluids*, **16**(5):1668–1693, May 2004.

[37] Jean Donea and Antonio Huerta. *Finite Element Methods for Flow Problems*. John Wiley and Sons, Hoboken, NJ, 2003.

[38] John K. Dukowicz and Bertrand J. A. Meltz. Vorticity errors in multidimensional lagrangian codes. *Journal of Computational Physics*, **99**(1):115–134, March 1992.

[39] Grant V. Farnsworth and Allen C. Robinson. Improved kinematic options in ALEGRA. Technical Report SAND2003-4510, Sandia National Laboratories, Albuquerque, NM, December 2003.

[40] D. P. Flanagan and T. Belytschko. A uniform strain hexahedron and quadrilateral with orthogonal hourglass control. *International Journal for Numerical Methods in Engineering*, **17**(5):679–706, 1981.

[41] D. P. Flanagan and L. M. Taylor. An accurate numerical algorithm for stress integration with finite rotations. *Computer Methods in Applied Mechanics and Engineering*, **62**(3):305–320, June 1987.

[42] Michel Fortin and Roland Glowinski. *Augmented Lagrangian Methods: Applications to the Numerical Solution of Boundary-Value Problems*, volume 15 of *Studies in Mathematics and its Applications*. North-Holland, New York, 1983.

[43] C. J. Garasi, D. E. Bliss, T. A. Mehlhorn, B. V. Oliver, A. C. Robinson, and G. S. Sarkisov. Multi-dimensional high energy density physics modeling and simulation of wire array z-pinch physics. *Physics of Plasmas*, **11**(5):2729–2737, May 2004.

[44] G. L. Goudreau and J. O. Hallquist. Recent developments in large-scale finite element lagrangian hydrocode technology. *Computer Methods in Applied Mechanics and Engineering*, **33**(1-3):725–757, September 1982.

[45] D. F. Griffiths and J. Lorenz. An analysis of the petrov galerkin finite element method. *Computer Methods in Applied Mechanics and Engineering*, **14**(1):39–64, April 1978.

[46] Morton E. Gurtin. Thermodynamics and stability. *Archive for Rational Mechanics and Analysis*, **59**(1):63–96, March 1975.

[47] Morton E. Gurtin. *An Introduction to Continuum Mechanics*. Academic Press, 1981.

[48] John O. Hallquist. *User's Manual for Dyna2D*. Lawrence Livermore Laboratory, Livermore, CA, January 1984. UCID 18756 Rev. 2.

[49] John O. Hallquist. LS-DYNA theoretical manual. Technical report, Livermore Software Technology Corporation, Livermore, CA, May 1998.

[50] Martin W. Heinstein, Frank J. Mello, Stephen W. Attaway, and Tod A. Laursen. Contact-impact modeling in explicit transient dynamics. *Computer Methods in Applied Mechanics and Engineering*, **187**(3-4):621–640, July 2000.

[51] Nicholas Higham. Computing the polar decomposition - with applications. *SIAM Journal on Scientific and Statistical Computing*, **7**(4):1160–1174, October 1986.

[52] Nicholas Higham and Robert Schreiber. Fast polar decomposition of an arbitrary matrix. *SIAM Journal on Scientific and Statistical Computing*, **11**(4):648–655, July 1990.

[53] Gerhard A. Holzapfel. *Nonlinear Solid Mechanics: A Continuum Approach for Engineering*. John Wiley & Sons, March 2000.

[54] Thomas Y. Hou and Philippe G. LeFloch. Why nonconservative schemes converge to wrong solutions: Error analysis. *Mathematics of Computation*, **62**(206):497–530, April 1994.

[55] T. J. R. Hughes, L. P. Franca, and M. Mallet. A new finite element formulation for computational fluid dynamics: I. Symmetric forms of the compressible euler and navier-stokes equations and the second law of thermodynamics. *Computer Methods in Applied Mechanics and Engineering*, **54**(2):235–243, February 1986.

[56] Thomas J. R. Hughes. *The Finite Element Method: Linear Static and Dynamic Finite Element Analysis*. Dover Publications, 2000.

[57] Thomas J. R. Hughes and James Winget. Finite rotation effects in numerical integration of rate constitutive equations arising in large-deformation analysis. *International Journal for Numerical Methods in Engineering*, **15**(12):1862–1867, December 1980.

[58] R. Hutter, P. Hora, and P. Niederer. Total hourglass control for hyperelastic materials. *Computer Methods in Applied Mechanics and Engineering*, **189**(3):991–1010, September 2000.

[59] E. S. Hertel Jr, R. L. Bell, M. G. Elrick, A. V. Farnsworth, G. I. Kerley, J. M. McGlaun, S. V. Petney, S. A. Silling, P. A. Taylor, and L. Yarrington. CTH: A software family for multi-dimensional shock physics analysis. In *Proceedings of the 19th International Symposium on Shock Waves*, pages 377–382, Marseille, France, July 1993.

[60] C. Kane, J. E. Marsden, M. Ortiz, and M. West. Variational integrators and the Newmark algorithm for conservative and dissipative mechanical systems. *International Journal for Numerical Methods in Engineering*, **49**(10):1295–1325, December 2000.

[61] Milos Kojic and Klaus-Jurgen Bathe. Studies of finite element procedures - stress solution of a closed elastic strain path with stretching and shearing using the updated lagrangian Jaumann formulation. *Computers and Structures*, **26**(1-2):175–179, 1987.

[62] T. A. Laursen, S. W. Attaway, and R. I. Zadoks. SEACAS theory manuals. Technical Report SAND98-1760/1-3, Sandia National Laboratories, P.O. Box 5800, Albuquerque, NM 87185, 1998. (`http://endo.sandia.gov/SEACAS/Documentation/SEACAS.html`).

[63] Peter Lax and Burton Wendroff. Systems of conservation laws. *Communications on Pure and Applied Mathematics*, **13**(2):217–237, May 1960.

[64] Peter D. Lax. *Hyperbolic Systems of Conservation Laws and the Mathematical Theory of Shock Waves*, volume 11 of *CBMS-NSF Regional Conference Series in Applied Mathematics*. SIAM(Society for Industrial and Applied Mathematics), Philidelphia, PA, 1972.

[65] B. Leavy, C. Krauthauser, J. Houskamp, and J. LaSalvia. Fundamental investigation of high-velocity impact of ductile projectiles on confined ceramic targets. In *Proceedings of the 25th Army Science Conference*, Orlando, FL, November 2006.

[66] R. W. Lemke, M. D. Knudson, A. C. Robinson, T. A. Haill, K. W. Struve, J. R. Asay, and T. A. Mehlhorn. Self-consistent, two-dimensional, magnetohydrodynamic simulations of magnetically driven flyer plates. *Physics of Plasmas*, **10**(5):1867–1874, May 2003.

[67] Randall J. Leveque. *Finite Volume Methods for Hyperbolic Problems*. Cambridge Texts in Applied Mathematics. Cambridge University Press, Cambridge, UK, 2002.

[68] Randall J. LeVeque. *Numerical Methods for Conservation Laws*. Lectures in Mathematics. Birkhauser, 2nd edition, February 2006.

[69] A. Lew, J. E. Marsden, M. Ortiz, and M. West. Variational time integrators. *International Journal for Numerical Methods in Engineering*, **60**(1):153–212, May 2004.

[70] Wing Kam Liu, Herman Chang, Jiun-Shyan Chen, and Ted Belytschko. Arbitrary lagrangian-eulerian petrov-galerkin finite elements for nonlinear continua. *Computer Methods in Applied Mechanics and Engineering*, **68**(3):259–310, June 1988.

[71] Jerrold E. Marsden and Thomas J. R. Hughes. *Mathematical Foundations of Elasticity*. Dover Publications, Mineola, NY, 1994.

[72] Jerrold E. Marsden and Tudor S. Ratiu. *Introduction to Mechanics and Symmetry*, volume 17 of *Texts in Applied Mathematics*. Springer, New York, 2nd edition, 1999.

[73] P. Matejovic and V. Adamik. A one-point integration quadrilateral with hourglass control in axisymmetric geometry. *Computer Methods in Applied Mechanics and Engineering*, **70**(3):301–320, October 1988.

[74] J. M. McGlaun, S. L. Thompson, and M. G. Elrick. A brief description of the three-dimensional shock wave physics code CTH. Technical Report SAND89-0607C, Sandia National Laboratories, Albuquerque, NM, July 1989.

[75] Ralph Menikoff and Bradley J. Plohr. The Riemann problem for fluid flow of real materials. *Reviews of Modern Physics*, **61**(1):75–130, January 1989.

[76] C. Miehe. Entropic thermoelasticity at finite strains. Aspects of the formulation and numerical implementation. *Computer Methods in Applied Mechanics and Engineering*, **120**(3-4):243–269, February 1995.

[77] G. H. Miller and P. Colella. A conservative three-dimensional eulerian method for coupled solid fluid shock capturing. *Journal of Computational Physics*, **183**(1):26–82, November 2002.

[78] W. F. Noh. Errors for calculations of strong shocks using an artificial viscosity and an artificial heat flux. *Journal of Computational Physics*, **72**(1):78–120, September 1987.

[79] R. W. Ogden. *Non-Linear Elastic Deformations*. Dover Publications, Mineola, NY, 1997.

[80] J. Michael Owen. A tensor artificial viscosity for SPH. *Journal of Computational Physics*, **201**(2):601–629, December 2004.

[81] James S. Peery and Daniel E. Carroll. Multi-material ALE methods in unstructured grids. *Computer Methods in Applied Mechanics and Engineering*, **187**(3-4):591–619, July 2000.

[82] Michael Anthony Puso. A highly efficient enhanced assumed strain physically stabilized hexahedral element. *International Journal for Numerical Methods in Engineering*, **49**(8):1029–1064, November 2000.

[83] R. Reiben. Mixed finite element methods for lagrangian hydrodynamics. Technical Report UCRL-PRES-231264, Lawrence Livermore National Laboratory, Livermore, CA, June 2007.

[84] W. Rider, G. Weirs, A. Robinson, C. Ober, E. Love, H. Hanshaw, R. Lemke, G. Scovazzi, J. Shadid, and J. Banks. Algorithm developments in Alegra guided by testing. Conference presentation, Numerical methods for multi-material fluid flows, Czech Technical University in Prague, September 10-14, 2007. Conference web site: http://www-troja.fjfi.cvut.cz/∼multimat07/.

[85] W. J. Rider, E. Love, and G. Scovazzi. A stability analysis of the Alegra lagrangian hydrodynamics method. Technical Report SAND-2007-7640C, Sandia National Laboratories, Albuquerque, NM, November 2007. Presented at the LLNL Workshop on Advanced Numerical Methods for Lagrangian Hydrodynamics, Livermore, CA, November 12-15, 2007.

[86] R. N. Rieben, G. H. Rodrigue, and D. A. White. A high order mixed vector finite element method for solving the time dependent maxwell equations on unstructured grids. *Journal of Computational Physics*, **204**(2):490–519, April 2005.

[87] R. N. Rieben, D. A. White, B. K. Wallin, and J. M. Solberg. An arbitrary lagrangian-eulerian discretization of MHD on 3d unstructured grids. *Journal of Computational Physics*, **226**(1):534–570, September 2007.

[88] Robert N. Rieben. Mixed finite element methods for lagrangian hydrodynamics. Conference presentation, Numerical methods for multi-material fluid flows, Czech Technical University in Prague, September 10-14, 2007. Conference web site: http://www-troja.fjfi.cvut.cz/∼multimat07/.

[89] Allen C. Robinson and Christopher J. Garasi. Three-dimensional z-pinch wire array modeling with ALEGRA-HEDP. *Computer Physics Communications*, **164**(1-3):408–413, December 2004.

[90] Samit Roy, Arlo F. Fossum, and Robert J. Dexter. On the use of polar decomposition in the integration of hypoelastic constitutive laws. *International Journal of Engineering Science*, **30**(2):119–133, February 1992.

[91] William D. Schulz. Tensor artificial viscosity for numerical hydrodynamics. *Journal of Mathematical Physics*, **5**(1):133–138, January 1964.

[92] G. Scovazzi, M. A. Christon, T. J. R. Hughes, and J. N. Shadid. Stabilized shock hydrodynamics: I. A Lagrangian method. *Computer Methods in Applied Mechanics and Engineering*, **196**(4-6):923–966, January 2007.

[93] G. Scovazzi, E. Love, and M. Shashkov. A multi-scale Q1/P0 approach to langrangian shock hydrodynamics. Technical Report SAND2007-1423, Sandia National Laboratories, Albuquerque, NM, 2007.

[94] G. Scovazzi, E. Love, and M. J. Shashkov. Multi-scale lagrangian shock hydrodynamics on Q1/P0 finite elements: Theoretical framework and two-dimensional computations. *Computer Methods in Applied Mechanics and Engineering*, **197**(9-12):1056–1079, February 2008. doi:10.1016/j.cma.2007.10.002.

[95] J. C. Simo, F. Armero, and R. L. Taylor. Improved versions of assumed enhanced strain tri-linear elements for 3D finite deformation problems. *Computer Methods in Applied Mechanics and Engineering*, **110**(3-4):359–386, December 1993.

[96] J. C. Simo and T. J. R. Hughes. *Computational Inelasticity*, volume 7 of *Interdisciplinary applied mathematics*. Springer, New York, 1998.

[97] J. C. Simo and C. Miehe. Associative coupled thermoplasticity at finite strains: Formulation, numerical analysis and implementation. *Computer Methods in Applied Mechanics and Engineering*, **98**(1):41–104, July 1992.

[98] J. C. Simo and K. S. Pister. Remarks on rate constitutive equations for finite deformation problems: computational implications. *Computer Methods in Applied Mechanics and Engineering*, **46**(2):201–215, October 1984.

[99] Randall M. Summers, James S. Peery, Michael K. Wong, Eugene S. Hertel, Timothy G. Trucano, and Lalit C. Chhabildas. Recent progress in Alegra development and application to ballistic impacts. *International Journal of Impact Engineering*, **20**(6-10):779–788, 1997.

[100] L. M. Taylor and D. P. Flanagan. Pronto 3d : A three-dimensional transient solid dynamics program. Technical Report SAND87-1912, Sandia National Laboratories, Albuquerque, NM, March 1989.

[101] J. W. Thomas. *Numerical Partial Differential Equations: Conservation Laws and Elliptic Problems*, volume 33 of *Texts in Applied Mathematics*. Springer-Verlag, New York, 1999.

[102] C. Truesdell. *Rational thermodynamics*. Springer-Verlag, New York, 2nd edition, 1984.

[103] C. A. Truesdell. Hypo-elasticity. *Journal for Rational Mechanics and Analysis*, **4**:83–133 & 1019–1020, 1955.

[104] C. A. Truesdell and W. Noll. *The non-linear field theories of mechanics*. Springer-Verlag, New York, 2nd edition, 1992.

[105] Efrem Vitali and David J. Benson. An extended finite element formulation for contact in multi-material arbitrary lagrangian-eulerian calculations. *International Journal for Numerical Methods in Engineering*, **67**(10):1420–1444, September 2006.

[106] J. VonNeumann and R. D. Richtmyer. A method for the numerical calculation of hydrodynamic shocks. *Journal of Applied Physics*, **21**(3):232–237, March 1950.

[107] F. Vander Weeen and T. Belytschko. Correction of article by D. P. Flanagan and T. Belytschko. *International Journal for Numerical Methods in Engineering*, **19**(3):467–468, 1983.

[108] Mark L. Wilkins. Use of artificial viscosity in multidimensional fluid dynamic calculations. *Journal of Computational Physics*, **36**(3):281–303, July 1980.

[109] M. K. Wong, J. R. Weatherby, C. D. Turner, A. C. Robinson, T. A. Haill, and D. E. Carroll. Physics applications in the Alegra framework. In K. J. Bathe, editor, *Proceedings of the First MIT Conference on Computational Fluid and Solid Mechanics*, Computational Fluid and Solid Mechanics, Cambridge, Massachusetts, June 2001. Massachusetts Institute of Technology, Elsevier.

[110] Joseph P. Wright. Numerical instability due to varying time steps in explicit wave propagation and mechanics calculations. *Journal of Computational Physics*, **140**(2):421–431, March 1998.

[111] Ya. B. Zel'dovich and Yu. P. Raizer. *Physics of Shock Waves and High-Temperature Hydrodynamic Phenomena*. Dover Publications, Mineola, NY, 2002.

[112] O. C. Zienkiewicz, R. L. Taylor, and J. Z. Zhu. *The Finite Element Method: Its Basis and Fundamentals*. Elsevier Butterworth-Heinemann, Burlington, MA, sixth edition, 2005.

A Proposed alternative energy update algorithm

This goal of this subsection is to present an alternative to the ALEGRA algorithm currently used for incremental energy updates. First, consider equation (63)

$$\rho_{\mathrm{t}}\dot{\varepsilon} = \boldsymbol{\sigma}_{\mathrm{t}} \bullet \mathbf{d}_{\mathrm{t}} \ .$$

By multiplying both side by J_{t} this equation may be written as

$$\rho_0\dot{\varepsilon} = \boldsymbol{\tau}_{\mathrm{t}} \bullet \mathbf{d}_{\mathrm{t}} \ . \tag{139}$$

The goal here is to write the above equation in a more convenient form for developing a consistent numerical approximation.

To begin developments, decompose the energy evolution equation into volumetric and deviatoric parts such that

$$\rho_0\dot{\varepsilon} = \bar{\tau} \cdot \operatorname{trace}\mathbf{d} \ + \ \operatorname{dev}\boldsymbol{\tau} \bullet \mathbf{d} \ , \tag{140}$$

where $\bar{(\cdot)} := \frac{1}{3}\operatorname{trace}(\cdot)$. Using the above developments and the fact that $\dot{J} = J \cdot \operatorname{trace}\mathbf{d}$ one can write

$$\rho_0\dot{\varepsilon} = \bar{\sigma} \cdot \dot{J} \ + \ \frac{1}{2}\boldsymbol{\varphi}^*(\operatorname{dev}\boldsymbol{\tau}) \bullet \dot{\mathbf{C}} \ . \tag{141}$$

Applying a generalized midpoint integrator to the equation yields

$$\rho_0(\varepsilon_{n+1} - \varepsilon_n) \cong \bar{\sigma}_{n+\beta} \cdot (J_{n+1} - J_n) \; + \; \frac{1}{2}\boldsymbol{\varphi}^*_{n+\beta}(\operatorname{dev}\boldsymbol{\tau}_{n+\beta}) \bullet (\mathbf{C}_{n+1} - \mathbf{C}_n) \quad \text{for} \quad \beta \in [0,1] \; . \tag{142}$$

One can use the developments in section 3.1 to expand this into

$$\left.\begin{aligned} \rho_0(\varepsilon_{n+1} - \varepsilon_n) &= \bar{\sigma}_{n+\beta} \cdot (J_{n+1} - J_n) \; + \; \frac{1}{2}\boldsymbol{\varphi}^*_{n+\beta}(\operatorname{dev}\boldsymbol{\tau}_{n+\beta}) \bullet (\mathbf{C}_{n+1} - \mathbf{C}_n) \\ &= \bar{\sigma}_{n+\beta} \cdot (j_{n+1} J_n - J_n) \; + \; \frac{1}{2}\boldsymbol{\varphi}^*_{n+\beta}(\operatorname{dev}\boldsymbol{\tau}_{n+\beta}) \bullet (\mathbf{F}_n^T \mathbf{f}_{n+1}^T \mathbf{f}_{n+1} \mathbf{F}_n - \mathbf{F}_n^T \mathbf{F}_n) \\ &= \bar{\sigma}_{n+\beta} \cdot (j_{n+1} - 1) J_n \; + \; \frac{1}{2}\mathbf{F}_n \boldsymbol{\varphi}^*_{n+\beta}(\operatorname{dev}\boldsymbol{\tau}_{n+\beta}) \mathbf{F}_n^T \bullet (\mathbf{f}_{n+1}^T \mathbf{f}_{n+1} - \mathbf{I}) \end{aligned}\right\} \; . \tag{143}$$

Next, define $\operatorname{DEV}(\mathbf{S}) := \boldsymbol{\varphi}^*(\operatorname{dev}\boldsymbol{\tau})$ and note that $\mathbf{F}_{n+\beta} = \mathbf{f}_{n+\beta}\mathbf{F}_n$. The discrete energy evolution equation can then be written as

$$\left.\begin{aligned} \rho_0(\varepsilon_{n+1} - \varepsilon_n) &= \bar{\sigma}_{n+\beta} \cdot (j_{n+1} - 1) J_n \; + \; \frac{1}{2}\mathbf{F}_n \boldsymbol{\varphi}^*_{n+\beta}(\operatorname{dev}\boldsymbol{\tau}_{n+\beta}) \mathbf{F}_n^T \bullet (\mathbf{f}_{n+1}^T \mathbf{f}_{n+1} - \mathbf{I}) \\ &= \bar{\sigma}_{n+\beta} \cdot (j_{n+1} - 1) J_n \; + \; \frac{1}{2}\mathbf{F}_n [\operatorname{DEV}\mathbf{S}_{n+\beta}] \mathbf{F}_n^T \bullet (\mathbf{f}_{n+1}^T \mathbf{f}_{n+1} - \mathbf{I}) \\ &= \bar{\sigma}_{n+\beta} \cdot (j_{n+1} - 1) J_n \; + \; \frac{1}{2}\mathbf{f}_{n+\beta}^{-1} \mathbf{F}_{n+\beta} [\operatorname{DEV}\mathbf{S}_{n+\beta}] \mathbf{F}_{n+\beta}^T \mathbf{f}_{n+\beta}^{-T} \bullet (\mathbf{f}_{n+1}^T \mathbf{f}_{n+1} - \mathbf{I}) \\ &= \bar{\sigma}_{n+\beta} \cdot (j_{n+1} - 1) J_n \; + \; \frac{1}{2}\mathbf{f}_{n+\beta}^{-1} \boldsymbol{\varphi}_{n+\beta_*} [\operatorname{DEV}\mathbf{S}_{n+\beta}] \mathbf{f}_{n+\beta}^{-T} \bullet (\mathbf{f}_{n+1}^T \mathbf{f}_{n+1} - \mathbf{I}) \\ &= \bar{\sigma}_{n+\beta} \cdot (j_{n+1} - 1) j_{n+\beta}^{-1} J_{n+\beta} \; + \; \frac{1}{2}\mathbf{f}_{n+\beta}^{-1} (\operatorname{dev}\boldsymbol{\tau}_{n+\beta}) \mathbf{f}_{n+\beta}^{-T} \bullet (\mathbf{f}_{n+1}^T \mathbf{f}_{n+1} - \mathbf{I}) \\ &= \bar{\sigma}_{n+\beta} \cdot (j_{n+1} - 1) j_{n+\beta}^{-1} J_{n+\beta} \; + \; \frac{1}{2} J_{n+\beta} \mathbf{f}_{n+\beta}^{-1} (\operatorname{dev}\boldsymbol{\sigma}_{n+\beta}) \mathbf{f}_{n+\beta}^{-T} \bullet (\mathbf{f}_{n+1}^T \mathbf{f}_{n+1} - \mathbf{I}) \end{aligned}\right\} \; . \tag{144}$$

Of course, conservation of mass requires that $\rho_0 = \rho_{n+\beta} J_{n+\beta}$ so

$$\rho_{n+\beta}(\varepsilon_{n+1} - \varepsilon_n) = j_{n+\beta}^{-1} \bar{\sigma}_{n+\beta} \cdot (j_{n+1} - 1) \; + \; \frac{1}{2}\mathbf{f}_{n+\beta}^{-1} (\operatorname{dev}\boldsymbol{\sigma}_{n+\beta}) \mathbf{f}_{n+\beta}^{-T} \bullet (\mathbf{f}_{n+1}^T \mathbf{f}_{n+1} - \mathbf{I}) \; . \tag{145}$$

Noting that $\rho_n = \rho_{n+\beta} j_{n+\beta}$, the above equation may be multiplied through by $j_{n+\beta}$, yielding

$$\boxed{\rho_n(\varepsilon_{n+1} - \varepsilon_n) = \bar{\sigma}_{n+\beta} \cdot (j_{n+1} - 1) \; + \; \frac{1}{2}\mathbf{f}_{n+\beta}^{-1} (\operatorname{dev} j_{n+\beta}\boldsymbol{\sigma}_{n+\beta}) \mathbf{f}_{n+\beta}^{-T} \bullet (\mathbf{f}_{n+1}^T \mathbf{f}_{n+1} - \mathbf{I}) \; .} \tag{146}$$

Remarks A.1.

1. The above algorithm is second-order accurate if and only if $\beta = 1/2$. For all other choices of β the algorithm is only first-order accurate.
2. For $\beta > 0$ the algorithm is implicit since typically the stress at time $t_{n+\beta}$ depends on the energy at both times t_n and t_{n+1}.
3. The algorithm is, by construction, incrementally objective for any choice of the parameter $\beta \in [0,1]$.
4. For a purely deviatoric deformation ($j_{n+1} = 1$), no volume-work is done. This property is ensured a-priori by the volumetric-deviatoric split.
5. With $\beta = 0$ the equation(s) are explicit. This very much simplifies the implementation as equation (146) reduces to
$$\rho_n(\varepsilon_{n+1} - \varepsilon_n) = \bar{\sigma}_n \cdot (j_{n+1} - 1) \; + \; \frac{1}{2} \operatorname{dev}\boldsymbol{\sigma}_n \bullet \mathbf{f}_{n+1}^T \mathbf{f}_{n+1} \; . \tag{147}$$
6. Unfortunately, when this energy update is used in conjunction with the central difference time stepping scheme, a conserved total energy quantity does not generally exist.

B Axisymmetric Formulations

B.1 Kinematics

Material cylindrical coordinates are generally denoted as $\{R, Z\}$, with R the radial coordinate and Z the axial coordinate. The corresponding spatial coordinates are denoted as $\{r, z\}$.

B.1.1 Deformation Gradient

The *deformation gradient* may be written in orthogonal cylindrical coordinates as

$$\mathbf{F} = \begin{bmatrix} \frac{\partial r}{\partial R} & \frac{\partial r}{\partial Z} & 0 \\ \frac{\partial z}{\partial R} & \frac{\partial z}{\partial Z} & 0 \\ 0 & 0 & \lambda_{\theta\theta} \end{bmatrix} , \tag{148}$$

where $\lambda_{\theta\theta} = r/R$ is the *hoop stretch*.

B.1.2 Volume Form(s)

The *volume form* transforms as

$$r \cdot dr \wedge dz = J \cdot R \cdot dR \wedge dZ , \tag{149}$$

where $J = \det \mathbf{F}$. The *area form* transforms as

$$dr \wedge dz = J \cdot \lambda_{\theta\theta}^{-1} \cdot dR \wedge dZ . \tag{150}$$

B.1.3 Deformation Rate

The *rate of deformation* tensor is defined as $\mathbf{d} = \mathrm{sym}(\dot{\mathbf{F}}\mathbf{F}^{-1})$.

B.2 Kinetics

B.2.1 "Area Galerkin"

The balance of linear momentum (in weak form) can be written as

$$\int \frac{\delta\varphi_r}{r} \left[\partial_r \sigma_{rr} + \frac{1}{r}(\sigma_{rr} - \sigma_{\theta\theta}) + \partial_z \sigma_{rz} + \rho b_r - \rho \dot{v}_r \right] r \cdot dr \wedge dz \ = 0 \quad \forall \delta\varphi_r , \tag{151a}$$

$$\int \frac{\delta\varphi_z}{r} \left[\partial_z \sigma_{zz} + \partial_r \sigma_{rz} + \frac{1}{r}\sigma_{rz} + \rho b_r - \rho \dot{v}_z \right] r \cdot dr \wedge dz \ = 0 \quad \forall \delta\varphi_z . \tag{151b}$$

This simplifies to

$$\int \delta\varphi_r \left[\partial_r \sigma_{rr} + \frac{1}{r}(\sigma_{rr} - \sigma_{\theta\theta}) + \partial_z \sigma_{rz} + \rho b_r - \rho \dot{v}_r \right] dr \wedge dz \ = 0 \quad \forall \delta\varphi_r , \tag{152a}$$

$$\int \delta\varphi_z \left[\partial_z \sigma_{zz} + \partial_r \sigma_{rz} + \frac{1}{r}\sigma_{rz} + \rho b_r - \rho \dot{v}_z \right] dr \wedge dz \ = 0 \quad \forall \delta\varphi_z . \tag{152b}$$

Integration by parts yields (omitting boundary terms)

$$\boxed{\int \left[\partial_r \delta\varphi_r \cdot \sigma_{rr} + \partial_z \delta\varphi_r \cdot \sigma_{rz}\right] dr \wedge dz \quad - \quad \int \delta\varphi_r \left[\frac{1}{r}(\sigma_{rr} - \sigma_{\theta\theta}) + \rho b_r - \rho \dot{v}_r\right] dr \wedge dz \; = 0 \quad \forall \delta\varphi_r \; ,} \tag{153a}$$

$$\boxed{\int \left[\partial_z \delta\varphi_z \cdot \sigma_{zz} + \partial_r \delta\varphi_z \cdot \sigma_{rz}\right] dr \wedge dz \quad - \quad \int \delta\varphi_z \left[\frac{1}{r}\sigma_{rz} + \rho b_r - \rho \dot{v}_z\right] dr \wedge dz \; = 0 \quad \forall \delta\varphi_z \; .} \tag{153b}$$

Remarks B.1.

1. This approach is advocated by [10, 44, 48].
2. Notice that the only difference between this formulation and a two-dimensional plane strain formulation is an extra term of the form $r^{-1}\sigma$ in the area integrals. All other integrals, including body force and surface traction, remain unchanged.
3. This is a *Petrov-Galerkin* [16, 45, 70] formulation since the weighting functions $\delta\varphi$ are scaled by the inverse radius r^{-1}, but the velocity (and position) interpolation functions are not.
4. Assume that the material model is a purely volumetric equation-of-state. In this situation $\sigma_{rz} = 0$ and $\sigma_{rr} = \sigma_{\theta\theta} = \sigma_{zz} = p$, where p is the thermodynamic pressure. The weak form(s) then simplify to

$$\int \partial_r \delta\varphi_r \cdot p \; dr \wedge dz \quad - \quad \int \delta\varphi_r \left[\rho b_r - \rho \dot{v}_r\right] dr \wedge dz \; = 0 \quad \forall \delta\varphi_r \; ,$$

$$\int \partial_z \delta\varphi_z \cdot p \; dr \wedge dz \quad - \quad \int \delta\varphi_z \left[\rho b_r - \rho \dot{v}_z\right] dr \wedge dz \; = 0 \quad \forall \delta\varphi_z \; .$$

   Notice that there are no "singular" (proportional to r^{-1}) terms in these integrals. This is the advantage of the "area Galerkin" formulation; it more easily allows for accurate numerical integration (quadrature) and thus produces (nearly) symmetric results for radially converging shocks [10]. Unfortunately, conservation and convergence properties may be negatively affected. See the immediately continuing remarks (5) and (6).
5. The algorithmic mass matrix for this formulation is not constant in time. This is easily verified by evaluating the integral

$$\left.\begin{aligned} \int \rho \cdot dr \wedge dz &= \int \rho_0 J^{-1} \cdot dr \wedge dz \\ &= \int \rho_0 J^{-1} \cdot J \lambda_{\theta\theta}^{-1} \cdot dR \wedge dZ \\ &= \int \rho_0 \, \lambda_{\theta\theta}^{-1} \cdot dR \wedge dZ \; . \end{aligned}\right\} \tag{154}$$

6. Since the algorithmic mass matrix is not constant, an energy conservation statement for this spatial algorithm is not readily available. One should not in general expect that total energy is discretely conserved. The lack of a conserved energy violates the assumptions of the Lax-Wendroff theorem [63, 101] and may in fact result in convergence to incorrect solutions [54].
7. This formulation is currently in Alegra .

B.2.2 Standard Galerkin

The balance of linear momentum (in weak form) can be written as

$$\int \delta\varphi_r \left[\partial_r \sigma_{rr} + \frac{1}{r}(\sigma_{rr} - \sigma_{\theta\theta}) + \partial_z \sigma_{rz} + \rho b_r - \rho \dot{v}_r\right] r \cdot dr \wedge dz \; = 0 \quad \forall \delta\varphi_r \; , \tag{155a}$$

$$\int \delta\varphi_z \left[\partial_z \sigma_{zz} + \partial_r \sigma_{rz} + \frac{1}{r}\sigma_{rz} + \rho b_r - \rho \dot{v}_z\right] r \cdot dr \wedge dz \; = 0 \quad \forall \delta\varphi_z \; . \tag{155b}$$

This may also be written as

$$\int (r\delta\varphi_r)\left[\partial_r\sigma_{rr}+\frac{1}{r}(\sigma_{rr}-\sigma_{\theta\theta})+\partial_z\sigma_{rz}+\rho b_r-\rho\dot{v}_r\right]dr\wedge dz\ =0\quad\forall\delta\varphi_r\ , \tag{156a}$$

$$\int (r\delta\varphi_z)\left[\partial_z\sigma_{zz}+\partial_r\sigma_{rz}+\frac{1}{r}\sigma_{rz}+\rho b_r-\rho\dot{v}_z\right]dr\wedge dz\ =0\quad\forall\delta\varphi_z\ . \tag{156b}$$

Integration by parts yields (omitting boundary terms)

$$\int [\partial_r(r\delta\varphi_r)\cdot\sigma_{rr}+\partial_z(r\delta\varphi_r)\cdot\sigma_{rz}]\,dr\wedge dz\quad-\quad\int r\delta\varphi_r\left[\frac{1}{r}(\sigma_{rr}-\sigma_{\theta\theta})+\rho b_r-\rho\dot{v}_r\right]dr\wedge dz\ =0\quad\forall\delta\varphi_r\ , \tag{157a}$$

$$\int [\partial_z(r\delta\varphi_z)\cdot\sigma_{zz}+\partial_r(r\delta\varphi_z)\cdot\sigma_{rz}]\,dr\wedge dz\quad-\quad\int r\delta\varphi_z\left[\frac{1}{r}\sigma_{rz}+\rho b_r-\rho\dot{v}_z\right]dr\wedge dz\ =0\quad\forall\delta\varphi_z\ . \tag{157b}$$

Expansion of the spatial derivatives and some algebraic manipulations results in

$$\boxed{\int [\partial_r\delta\varphi_r\cdot\sigma_{rr}+\partial_z\delta\varphi_r\cdot\sigma_{rz}]\,r\cdot dr\wedge dz\ -\ \int\delta\varphi_r\left[-\frac{1}{r}\sigma_{\theta\theta}+\rho b_r-\rho\dot{v}_r\right]r\cdot dr\wedge dz\ =0\quad\forall\delta\varphi_r\ ,} \tag{158a}$$

$$\boxed{\int [\partial_z\delta\varphi_z\cdot\sigma_{zz}+\partial_r\delta\varphi_z\cdot\sigma_{rz}]\,r\cdot dr\wedge dz\quad-\quad\int\delta\varphi_z\,[\rho b_r-\rho\dot{v}_z]\,r\cdot dr\wedge dz\ =0\quad\forall\delta\varphi_z\ .} \tag{158b}$$

Remarks B.2.

1. This approach can be considered standard in the finite element literature [56, 73, 112].
2. In this formulation, all integrals are radius-weighted. Volume integrals use the volume form $r\cdot dr\wedge dz$ and boundary traction integrals use the form $r\cdot ds$, where ds is the standard arc length form on curves (smooth sub-manifolds) in $\mathbb{R}^2$.
3. The (algorithmic) mass matrix for this formulation is constant in time. A conserved total energy quantity is thus easily defined, and in fact is the same as in section 5.3.2.
4. The error in numerical integration (quadrature) for this spatial approximation is not a secondary consideration. For example, elements closer to the z-axis (where $r=0$) have less mass than elements farther from that axis. This is due to the radial-weighting of the volume form in the integrals. Standard Gaussian quadrature, optimized for polynomial integration, may not be optional in this situation due to multiple terms containing the functions r and r^{-1}. Obviously, the symmetry of radially converging shocks can be affected by integration error.
5. For hyperelastic material models, this system of equations can be derived as the Euler-Lagrange equations of the Lagrangian
$$\mathsf{L}\ =\ \frac{1}{2}\int\rho_0\|\mathbf{v}\|^2R\cdot dR\wedge dZ\ -\ \int W\big(\mathbf{F}^T\mathbf{F}\big)\,R\cdot dR\wedge dZ\ , \tag{159}$$
for a suitably chosen (polyconvex) energy density function W.

C One-dimensional System of Equations

This appendix explicitly documents the ALEGRA system of equations in one(1) space dimension using a finite difference notation. In that regard, the notation $(\cdot)_j^n$ is meant as quantity $(\cdot)$ at time index n and space index j. Note also that

$$(\cdot)_{j+1/2}=\frac{1}{2}\left[(\cdot)_j+(\cdot)_{j+1}\right]\ .$$

The (constant) time step is denoted as $\Delta t>0$ and an ideal gamma-law gas material model is assumed. The "element" masses (constant in time) are notated as $m_j>0$. Also, x is position, u is velocity, e is internal energy and p is pressure.

C.1 Position

$$x_{j+1/2}^{n+1} = x_{j+1/2}^{n} + \Delta t u_{j+1/2}^{n+1/2} \tag{160}$$

$$h_j^n := x_{j+1/2}^{n} - x_{j-1/2}^{n} \tag{161}$$

C.2 Momentum

$$\frac{1}{\Delta t} m_{j+1/2}(u_{j+1/2}^{n+1/2} - u_{j+1/2}^{n-1/2}) + (p_{j+1}^n - p_j^n) = 0 \tag{162}$$

C.3 Energy

$$\frac{1}{\Delta t} m_j (e_j^{n+1} - e_j^n) \; + \; \frac{1}{2}\left[(u_{j+1/2}^{n+1/2} + u_{j+1/2}^{n-1/2}) - (u_{j-1/2}^{n+1/2} + u_{j-1/2}^{n-1/2})\right] p_j^n = 0 \tag{163}$$

C.4 Equation of State

$$p_j^n = (\gamma - 1)\frac{m_j}{h_j^n} e_j^n \tag{164}$$

C.5 Conservation

There are N elements numbered $\{0, 1, \cdots, N-1\}$. There are $(N+1)$ nodes numbered $\{-1/2, 1/2, \cdots, N-1/2\}$.

$$\frac{1}{2}\sum_{j=0}^{N} m_{j-1/2}\left\|u_{j-1/2}^{n+1/2}\right\|^2 \; + \; \sum_{j=0}^{N-1} m_j e_j^{n+1} \quad = \quad \frac{1}{2}\sum_{j=0}^{N} m_{j-1/2}\left\|u_{j-1/2}^{n-1/2}\right\|^2 \; + \; \sum_{j=0}^{N-1} m_j e_j^{n} \tag{165}$$

D Adiabatic Expansion of an Ideal Gas

Consider an ideal gas with initial (reference) properties: density $\rho_0 = 3220.0$, temperature $\Theta_0 = 4730.0530$, adiabatic exponent $\gamma = 5.0/3.0$ and specific heat at constant volume $C_v = 1000.0$. The gas is initially at rest in the two-dimensional domain $[-0.005, 0.005] \times 5120^{-1}[-0.5, 0.5]$. The domain is meshed with 5120×1 four-node quadrilateral elements. (This is one(1) row of square elements.) All the nodes of the mesh are constrained so that they cannot move in the x_2 direction. All the nodes, including those at the x_1 coordinates ± 0.005, are free to move in the x_1 direction. Zero(0) tractions are applied on the boundaries at $x_1 = \pm 0.005$. When released, the gas should undergo a rapid adiabatic (isentropic) expansion, with a rarefaction wave propagating inward from the outer edges of the domain [29].

The ALEGRA simulation results for this problem are shown in Figure D.1. Note the oscillations in the curve of pressure versus position. Density and velocity plots exhibit similar oscillations. This represents an apparent instability, since (entropy satisfying) rarefaction waves are (almost everywhere) smooth and non-oscillatory [67, 68, 111].

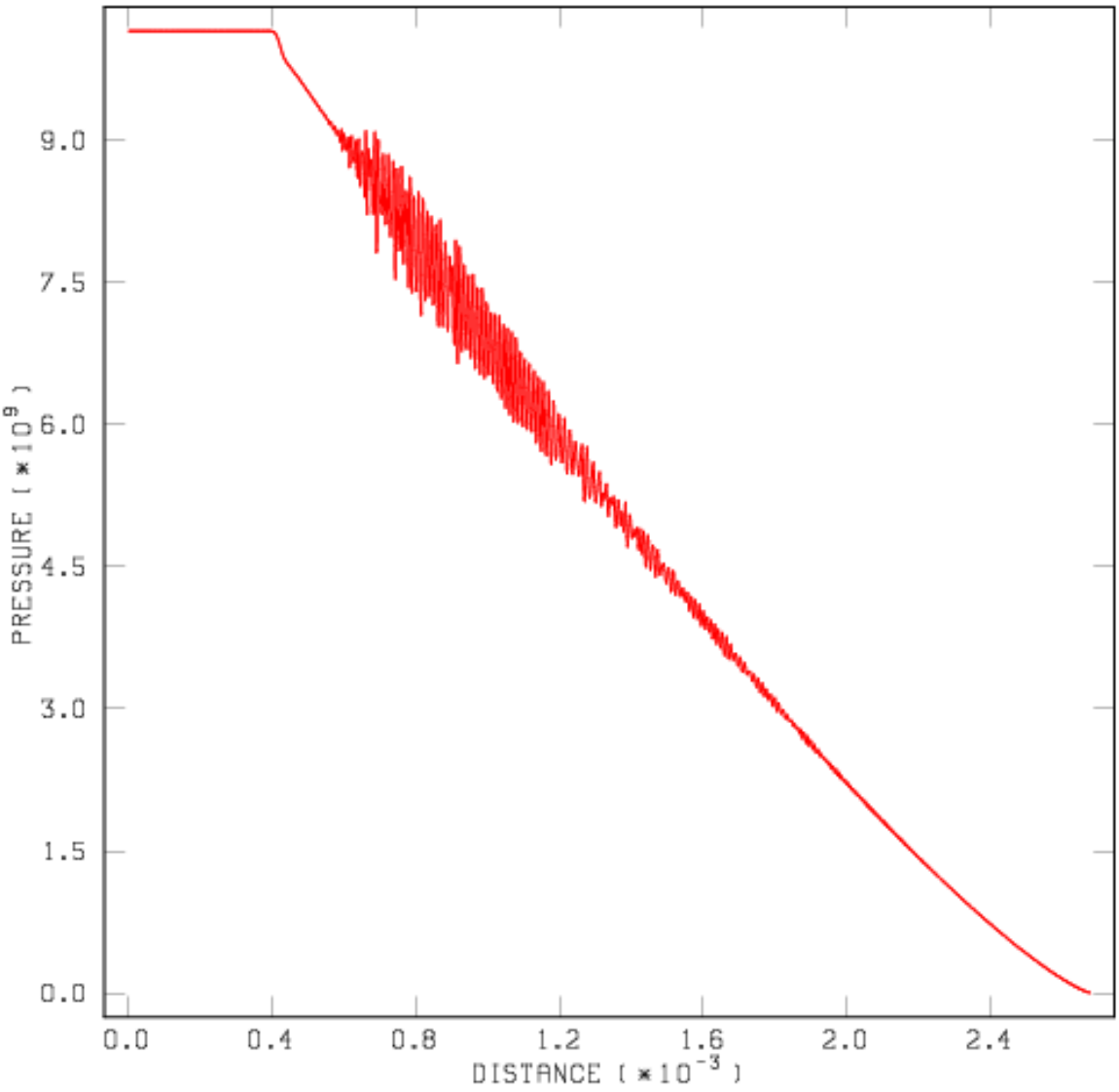

Figure D.1. pressure vs. position for adiabatic gas expansion

DISTRIBUTION:

1 Robert Doney
US Army Research Laboratory
AMSRD-ARL-WM-TA
Aberdeen Proving Ground, MD 21005-5066

1 Brian Leavy
US Army Research Laboratory
AMSRD-ARL-WM-TA
Aberdeen Proving Ground, MD 21005-5066

1 Robert N. Rieben
Scientific B-Division
Lawrence Livermore National Laboratory
7000 East Ave., L-095
Livermore, CA 94551

1 Mikhail Shashkov
Theoretical Division, Group T-7
MS-B284
Los Alamos National Laboratory
Los Alamos, NM 87545

1 MS 1318
James R. Stewart, 1411

1 MS 1320
Denis Ridzal, 1411

1 MS 0370
Timothy G. Trucano, 1411

1 MS 1320
Pavel B. Bochev, 1414

1 MS 1320
David M. Day, 1414

1 MS 1320
Richard B. Lehoucq, 1414

1 MS 1320
S. Scott Collis, 1416

1 MS 0378
Randall M. Summers, 1431

1 MS 0378
Richard R. Drake, 1431

1 MS 0378
David M. Hensinger, 1431

1 MS 0378
Marlin E. Kipp, 1431

1 MS 0378
Duane A. Labreche, 1431

1 MS 1319
Edward Love, 1431

1 MS 0378
Stewart J. Mosso, 1431

1 MS 0378
John Niederhaus, 1431

1 MS 0378
Sharon J. V. Petney, 1431

1 MS 0378
William J. Rider, 1431

1 MS 0378
Allen C. Robinson, 1431

1 MS 1319
Guglielmo Scovazzi, 1431

1 MS 0378
O. Erik Strack, 1431

1 MS 0378
V. Gregory Weirs, 1431

1 MS 0378
Michael K. Wong, 1431

1 MS 0370
James H. Strickland, 1433

1 MS 0316
Curtis C. Ober, 1433

1 MS 0378
Thomas E. Voth, 1433

1 MS 1322
John H. Carpenter, 1435

1 MS 1322
Joshua Robbins, 1435

1 MS 1322
Paul A. Taylor, 1435

1 MS 0316
John N. Shadid, 1437

1 MS 1322
Jeffrey W. Banks, 1437

1 MS 0380
Arne S. Gullerud, 1542

1 MS 0380
Martin Heinstein, 1542

1 MS 1186
Thomas A. Brunner, 1641

1 MS 1186
Kyle R. Cochrane, 1641

1 MS 1186
Christopher J. Garasi, 1641

1 MS 1186
Thomas A. Haill, 1641

1 MS 1186
Heath L. Hanshaw, 1641

1 MS 1186
Raymond W. Lemke, 1641

3 MS 9018
Central Technical Files, 8944

2 MS 0899
Technical Library, 4536

1 MS 0619
Review & Approval Desk, 9612